A validation of metabolic energy models in arm reaching

Garrick Bruening[1], Alaa Ahmed[2]

1 Integrative Physiology, University of Colorado Boulder, Boulder, Colorado, United States
2 Mechanical Engineering, University of Colorado Boulder, Boulder, Colorado, United States

* Garrick.Bruening@Colorado.edu

Abstract

Reaching movements are remarkably similar across healthy individuals. If one considers the selection of a movement as a result of a process that seeks to minimize a cost function, then the similarity of our movements would suggest that this cost function is conserved across individuals. Metabolic costs likely play a role in this cost function and ultimately in determining reach kinematics. However, computational models of reaching that seek to explain movement selection often resort to relying on a representation of movement effort rather than empirical metabolic measurements. These representations can take the form of models of metabolic cost or more general models of effort. Here we evaluate how a range of metabolic and effort models can predict empirical metabolic rate of reaching data. Metabolic rate was measured in subjects as they made arm reaching movements at six speeds while holding four added masses. A neuromechanical model of the arm was developed to calculate metabolic and effort representations using common metabolic and effort models. These metabolic and effort estimates were then compared to the empirical data. The best linear fit to the measured metabolic rate was Margaria's metabolic model with an R^2 value of 0.615, with three other metabolic models providing similar predictive power. Of the neuromechanical effort representations, work and work rate provided a comparable relation to metabolic rate (R^2=0.596, R^2=0.638). Rate of joint torque squared, a common measure of effort in reaching, was a poor fit comparatively to the metabolic data. The metabolic representations tended to capture the observed linear effect of mass on metabolic rate and the non-zero metabolic offset, whereas the effort models tended to overestimate the effect of mass on metabolic cost and not produce an offset. Our analysis highlights the importance of exercising caution when representing metabolic rate via model-derived biomechanical variables.

Introduction

When walking down the street, one may notice the surprising similarity in how everyone walks. When reaching for a cup of coffee, people will make very similar, straight, reaching movements. Every day we make hundreds of movements and somehow across the population these movements look very similar [1]. Because of this similarity, it has been proposed that there are costs to making a movement that humans attempt to minimize and that these costs are conserved across individuals [1, 2, 3]. In walking the primary cost is thought to be the metabolic energy cost to contract muscles, while in other movements it has taken many forms from metabolic energy to various measures of effort derived from neuromechanical variables [4, 5, 6, 7, 8].

Humans prefer to walk at the metabolically optimal speed and choose metabolically optimal gait patterns [7, 2, 9]. This has led to researchers to investigate metabolic cost as an explanatory variable in many types of movements. However, metabolic cost can be difficult to measure in some circumstances, which has led to the use of estimations of metabolic cost based on more easily derived variables. Metabolic cost has been represented as work done on center of mass, total joint work, active muscle volume, and recently direct estimates of metabolic cost from muscle-based energetics models. These models generally explain some, but not all, of the changes in metabolic cost [10, 11, 5, 12, 13].

In arm reaching, it is less clear what the cost is. With the importance of metabolic cost in walking, researchers have begun to investigate metabolic cost in arm reaching [6, 14]. Additionally, previous research has pointed toward this cost being some form of effort. Effort in arm reaching has been represented by many neuromechanical measures including joint torque, muscle force, muscle active state, and neural drive [15, 1, 16, 17, 14, 8]. Although the measurement of metabolic cost in arm reaching is relatively recent, it has been proposed that metabolic cost is a reasonable representation of effort [6]. In the case of arm reaching and novel or difficult movements, it can be difficult to measure metabolic cost due to the nature of the task or requiring repetition of the task. Therefore, it would be useful to know how well metabolic models and various effort representations can predict the empirically measured metabolic cost of reaching.

Within movement studies, there have been many ways researchers have represented metabolic cost and effort with the goal of predicting movement trajectories [8, 13, 18]. Metabolic cost models can range from sum of the torques about each joint to estimating the liberation of mechanical energy in muscles [16, 19, 20, 21, 22, 23, 24, 25, 26]. Estimates of effort in arm reaching are similar, but do not rely on estimating a metabolic rate, rather focus on some intrinsic property of the muscle or joints such as torque rate squared [27, 28], muscle active state [12, 16, 29], and neural stimulation [17]. Muscle energetic models have been used to simulate movements and to explain changes in metabolic cost for many locomotion studies [30, 31, 32, 13, 12, 19, 23]. These simulations have shown that they can reasonably reproduce movement trajectories similar to human subjects [33, 34, 35, 36, 37, 34, 38]. These models minimize some estimate of metabolic cost or effort (torque, jerk, muscle activation, etc.) to reproduce the human-like movements. While many of these estimates of metabolic cost can reproduce human-like movements, there are times where these functions fail. Humans, after being shown and trained on a curved path that minimizes a simulated metabolic cost, tend to reach in straight lines instead [39]. While this study points that subjects may not be minimizing solely metabolic cost, it may also mean that the metabolic model is not complete. This shows that depending on the metabolic representation used, one may not be able recreate realistic movements or make accurate predictions about the simulated cost of the movements, leading to the question of how accurately these models estimate metabolic cost of a movement.

These effort and metabolic models have become commonplace in movement simulation and in biomechanics research, however the validation for full body motion is still lacking. Recently, researchers have shown the relationship between simulated metabolic cost and actual metabolic cost in walking across many metabolic models [13, 18]. These studies show varying degrees of success using metabolic energy models to estimate collected metabolic data. Miller et al. show that the energy models predict widely varying metabolic costs [13]. Koelewijn et al. expanded on this by adding different speeds and slopes and found similar results; these estimations of metabolic cost have reasonable predictions but sometimes wide-ranging estimates for metabolic cost [18]. This type of validation has yet to be done for arm reaching and with many

representations of effort and metabolic cost in reaching, it is important to understand the relationship between these effort and metabolic representations and metabolic cost.

Here we develop a neuromechanical model of the arm performing a reaching movement that allows us to calculate estimates of metabolic cost using five different models of metabolic rate and compare these to collected metabolic data [19, 21, 23, 24, 40]. In addition, we compare seven neuromechanical effort representations to collected metabolic data. This analysis will inform us how well these metabolic and neuromechanical effort representations and neuromechanical are able to explain the metabolic cost of arm reaching.

Materials and methods

To investigate these questions, we collected metabolic and kinematic data as subjects made planar reaching movements across a range of speeds, distances, and while holding different amounts of mass at the hand. Next, we developed a neuromechanical model of the arm, and based on the measured movement kinematics used inverse dynamics to estimate the required shoulder and elbow torques for the movements, as well as additional neuromechanical variables of interest that have been used to represent effort: absolute joint torques, absolute joint torque rate, absolute joint work, absolute joint work rate, muscle force, muscle active state, and neural drive. To answer our first question of whether metabolic rate models (i.e.,metabolic representations) could capture the measured metabolic rate of reaching, we used five metabolic rate models to estimate the metabolic rate of the reaching movements and compared these estimates to the actual metabolic data collected experimentally. To answer our second question of how well alternative neuromechanical measures of effort represent metabolic rate (i.e.,effort representations), we compared the calculated absolute joint torques, absolute joint torque rate, absolute joint work, absolute joint work rate, muscle force, muscle active state, and neural drive to the measured metabolic rate. Details of the data collection, and calculations of the metabolic rate and neuromechanical effort representations are described below.

Experimental Protocol

Seated subjects made a series of planar horizontal arm reaching movements while breathing into a metabolic cart (Parvo Medics TrueOne 2400) and holding the handle of a robotic arm that supported their arm against gravity (Interactive Motion Technologies, Shoulder-Elbow Robot 2). Five male and three female subjects completed the experiment (all right-handed, mean age 28.9 years (std = 5.7), mean weight 68.4 kg (std = 11.4), and mean height 174.1 cm (std = 10.2). Subjects completed a set of arm reaching movements across eight targets, seven speeds, and four masses. All subjects gave written informed consent approved by the CU Boulder Institutional Review Board.

Subjects made reaches for a total of approximately 5 minutes while collecting metabolic data. Four different physical masses were added at the hand while subjects reached (0 kg, 2.27 kg, 4.55 kg, and 9.09 kg). The seven tested durations were: Very, Very Slow (VVS, 1.3 s, 160 trials), Very Slow (VS, 1.1 s, 170 trials), Slow (S, 0.9 s, 200 trials), Medium (M, 0.7 s, 220 trials), Fast (F, 0.5 s, 240 trials), Very Fast (VF, 0.375s, 250 trials), and Very, Very Fast (VVF, 0.25s, 260 trials). Conditions were blocked and randomized for each subject with each taking approximately five minutes. Every subject completed at least six speeds with each mass, where the two heavier masses were completed at the six slower speeds and the two lighter masses were completed at the six faster speeds. Four subjects did not complete the fastest speed with the lightest

two mass conditions, and two of these completed the slowest with the lightest mass, and two other subjects completed the slowest condition with the second lightest mass.

Subjects controlled a cursor on a screen positioned slightly above eye level about two feet away by moving the handle of the robotic arm. Subjects began the experiment by holding the cursor in a home circle for 200 ms. The home circle would then disappear, and a target would randomly appear at 45°, 135°, 225°, and 315° from the right horizontal (fig. 1A). Subjects were instructed to finish the movement within one of seven distinct 100 ms time windows such as completing the movement between 850 ms and 950 ms. Visual and auditory feedback was provided depending on if the movement was too fast, too slow, or within the time window. After completing the first reach (an outward reach), the target would be replaced with a new home circle and a second target would then appear in the central location after holding the cursor in the new home circle for 200 ms. This led to four outward reaching directions, and 4 inward reaching directions, for a total of 8 reaching movements. The location of the target in the outward reach would appear in a pseudorandom order, requiring a reach to four different targets then repeating another pseudorandom set. The X-Y position of the hand was recorded at 200 Hz and then filtered with a lowpass Butterworth filter (cutoff frequency 10 Hz). Custom MATLAB scripts were used to parse the data by trial, mass, and speed. The positional data was differentiated using a double five-point differentiation to compute velocity and acceleration, which were used to calculate movement duration and reaction time.

Subjects were instructed to be well-rested and fasted before metabolic testing. When subjects entered the lab, they remained seated in the testing chair for 10 minutes. Three baseline recording of metabolic rate were then taken for 5 minutes each before reaching began. Subjects then began making reaching movements in one of the block conditions. Between each block subjects had a five-minute rest period to adjust back to baseline. Based on the measured rates of oxygen consumption and carbon dioxide production, the metabolic power, $\dot{e}$, was calculated in joules per second using the method described by Brockway (eq. 1) [41].

$$\dot{e} = 16.58\dot{V}_{O_2} + 4.51\dot{V}_{CO_2} \tag{1}$$

Gross metabolic rate was calculated for each subject and each condition based on the last three minutes of reaching in each block. The average of the three baseline metabolic rates was subtracted from gross metabolic rate to determine the metabolic rate associated with the reaching movement alone.

Neuromechanical Model

A neuromechanical model of the arm was developed that includes the forearm and upper arm along with 8 physiologically relevant muscles crossing the shoulder and elbow joints (fig. 1B). This model is described in detail in the supplemental (sec S1). The masses and lengths of the arm were scaled by the subjects' height and weight and estimated using anthropomorphic measurements [29, 18, 42]. This led to heavier and taller subjects having heavier arms to move. Arm and muscle properties are described in detail in the supplemental information (arm - S1, muscles - S1).

The X-Y position data was re-sampled to 100 data points for each experimental arm reach then averaged at each new re-sampled time point for each subject, mass, speed, and target (supplemental S1). Position data was then used to calculate joint angles, which were differentiated using double five-point differentiation to compute joint velocities and accelerations. Joint position, velocity, and acceleration were in turn used to calculate joint torques using inverse dynamics on a per subject basis (supplemental S1). We then compute the muscle force for each muscle to match the computed joint

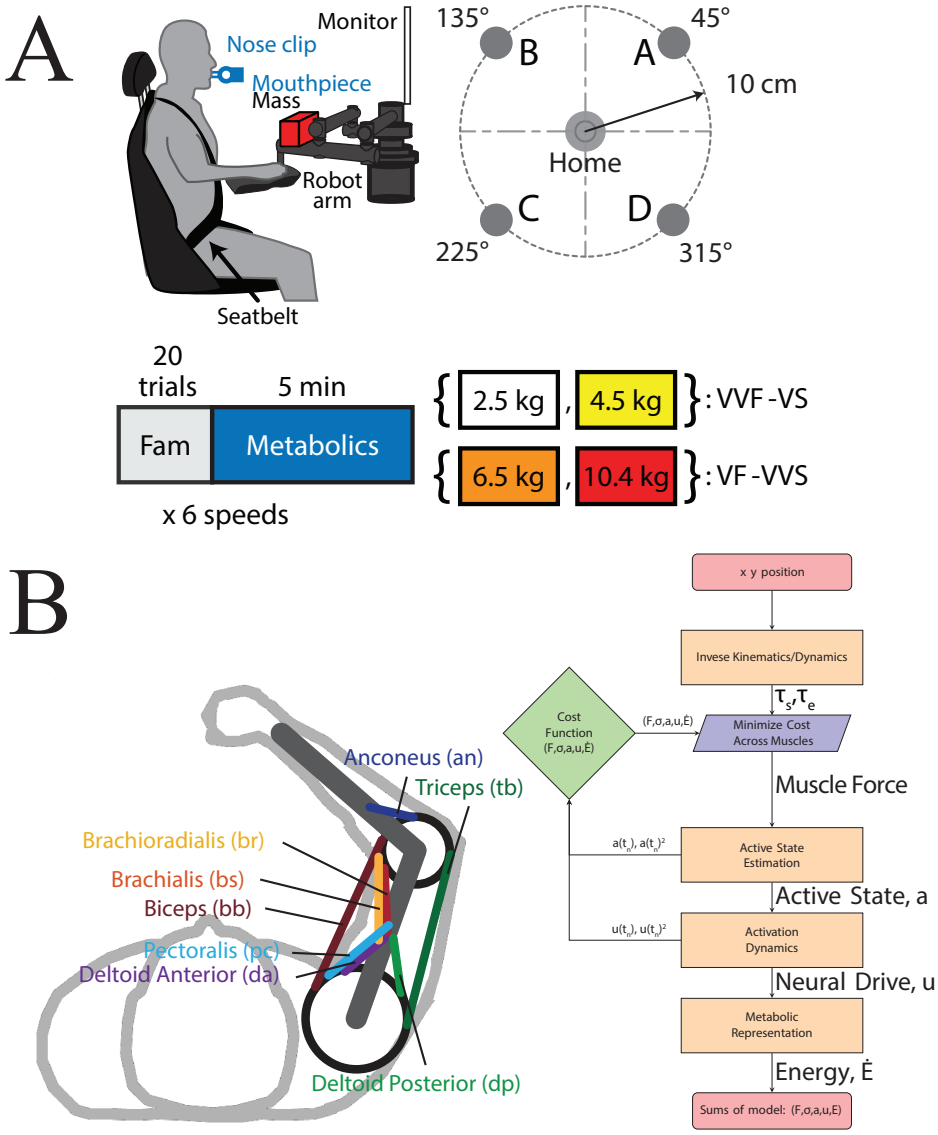

Fig 1. Description of experimental protocol and arm model. A. Subjects were in a seated position while collecting metabolic data. Mass was placed on a robotic manipulandum that subjects would hold onto that positioned the arm in approximately the horizontal plane. Subjects would make reaching movements to four different targets at six different speeds with four different masses added to their hands. B. Neuromechanical model of the arm with two joints and eight muscles. C. A flow chart describing calculation of metabolic and neuromechanical effort representation.

torques by optimizing one of nine possible objective (minimization) functions (supplemental S1).

Once muscle force was determined, we calculated muscle active state and neural drive. To compute muscle active state, we estimated the force-length and force-velocity properties of each muscle and found the active state required to produce the given muscle force (supplemental S1) [43]. After active state was estimated, a first order differential equation was used to calculate neural drive that estimates the active state rate as a function of neural drive (supplemental S1) [44, 17, 20, 45, 43, 46]. Thus, this model allowed us to calculate the seven neuromechanical representations of effort we sought to compare with metabolic rate: absolute joint torques, absolute joint torque rate, absolute joint work, absolute joint work rate, muscle force, muscle active state, and neural drive and their squared counterparts. We validated the neuromechanical models' inverse simulation by using the calculated neural drive to run model simulations in the forward direction and comparing the simulated movement trajectories to the experimentally measured trajectories (fig. S2).

Metabolic Representations

We calculated five metabolic rate estimates from the neuromechanical model (supplemental S1) [19, 23, 24, 21, 25]. The Umberger [19], Bhargava [21], Uchida [23], and Lichtwark [24] models all calculate energy rate ($\dot{E}$) as a summation of heat rates of the activation ($\dot{h_a}$), maintenance ($\dot{h_m}$), and shortening ($\dot{h_s}$) and lengthening ($\dot{h_l}$) of the contractile element and the total work rate ($\dot{w}$), with subtle differences in how each of the heat rates are calculated.

$$\dot{E} = \dot{h}_a + \dot{h}_m + \dot{h}_{sl} + \dot{w} \tag{2}$$

The activation heat rate is calculated as the energy required to initiate contraction of the muscle and is related to the neural drive and active state. The maintenance heat rate reflects the cost of keeping the muscle activated and depends on the active state and neural drive. The shortening and lengthening heat rates depend on the force-length and force-velocity properties of the muscle as well as the active state of the muscle. The work rate of the muscle is approximately the mechanical work done by or on the muscle.

The Margaria model [40] estimates the metabolic rate assuming that muscles are 25% efficient when shortening and 120% efficient while lengthening:

$$\dot{E} = \begin{cases} \frac{\dot{w}}{0.25} & \text{if } v_{CE} < 0 \\ -\frac{\dot{w}}{1.20} & \text{if } v_{CE} \geq 0 \end{cases} \tag{3}$$

Quantifying relationship to metabolic rate

The time series data for each of these metabolic and neuromechanical effort representations was integrated and averaged over all reaches (eight different reach types) to get an estimate of cost for each subject, mass, and speed condition. The metabolic and effort representations were then divided by the movement duration to get an estimate of the average metabolic rate over the movement. This rate was then fit to collected metabolic rate data using simple linear regression [47]. A fit was performed for each predictor variable and each objective function. For each variable we determined the significance of the slope and fits were ranked by the variance accounted for (R^2). A similar analysis comparing metabolic calculations and collected metabolic data in walking used a repeated measures correlation (RMCORR) to account for inter-subject variability [18]. In our analysis, we scale the size of the biomechanical model to the size

of each subject to account for the variability. We also complete our primary analysis using RMCORR to find if RMCORR predicts different results.

We also sought to parameterize the metabolic and effort representations in order to better describe how these representations varied as a function of mass and duration. We fit a parametric effort model with four free parameters to the measured metabolic rate, the five metabolic representations, and each neuromechanical effort representation (eq. 4) [6]. The general form of this equation has been shown to characterize the metabolic rate of both reaching and walking [6]. The metabolic or effort representation is indicated by $\dot{e}$, a is an offset term, b a scaling factor, c determines the scaling due to mass, and d determines the scaling due to time. The effective mass of the arm is m and is calculated on a subject specific basis and is described in detail in the supplemental information (sec S1) [6]. Total movement duration is represented by T.

$$\dot{e} = a + \frac{bm^c}{T^d} \tag{4}$$

After computing the best parameter fits, we compared the parameters to the metabolic data using equation 5 [48] where SE represents the standard error of the mean. If this inequality is true, there would be a significant difference between parameter estimates. In our study, we are interested in parameters that are not significantly different than the parameters fit to the measured metabolic data.

$$|mean_A - mean_B| > 2\sqrt{(SE_A^2 + SE_B^2)} \tag{5}$$

Comparing metabolic and predicted estimate distributions

Because our metabolic data is not evenly distributed (skew = 1.205, Shapiro-Wilk test p = 3.049) and has many low cost values and few high cost values, the use of R^2 may not be the best method to determine accuracy. We performed further analysis that compared the distribution of predictions to the metabolic data and determined if the two distributions were similar. For each variable including experimental metabolic power, we normalized each value to the maximum possible value for that metric. This gave us a distribution of experimental and predicted values between 0 and 1. We then computed the total difference in densities of every representation and experimental metabolic power and also used a Kolmogorov–Smirnov test (KS test) to determine if the predicted distributions differed from the experimental metabolic power distribution.

Results

We developed a neuromechanical model of the human arm and simulated reaches with four different masses, at six different speeds, and towards four targets. We then calculated seven different neuromechanical effort representations (absolute joint torques, absolute joint torque rate, absolute joint work, absolute joint work rate, muscle force, muscle active state, and neural drive and their squared counterparts) and five different metabolic estimates for the metabolic rate of each movement. These candidate representations were then compared to collected metabolic rate data for each movement and we determined how metabolic rate and each of these candidate representations are affected by added mass and movement duration.

The relation between metabolic energy models and metabolic rate

The primary goal of this study is to determine the relationship between the measured metabolic rate and each of the model-derived metabolic calculations. We performed linear regression between the metabolic representation and metabolic rate, and computed the variance accounted for (R^2, Tab. 1, Fig 2A). Across all metabolic representations, the Margaria energy model performed the best with an R^2 value of 0.615 when minimizing neural drive (Fig. 2B). The relative performance of the metabolic representations and neuromechanical representations remained the same regardless of the minimization function used for muscle force distribution (Fig. 2B). Since minimizing neural drive produced the highest overall R^2 value, all results presented are based on a muscle force distribution function that minimizes neural drive.

The best linear fit to measured metabolic rate was obtained using the Margaria energy expenditure model (Fig. 3, $R^2 = 0.615$, $y = 2.04x + 25.1$). The Uchida ($R^2 = 0.599$), Bhargava ($R^2 = 0.567$), and Umberger model ($R^2 = 0.543$) had comparatively high R^2 values. The Lichtwark model performed poorly compared to the other metabolic representations ($R^2 = 0.393$).

These models provide a general linear relationship to metabolic rate, but many show a trend of not being able to predict the metabolic rate of fast movements with low mass (Fig. 3). This can be seen in the data points far above the regression line, and generally near the top left of the graph. Specifically, the measured metabolic rate for a fast 0 kg and 2.27 kg movement is much greater than that predicted by any of the metabolic models. The Lichtwark and Margaria models exemplify this, as the 0 kg metabolic data is greater at the higher speeds than either metabolic representation predicts (Fig. 3).

We can also compare the ability of each representation to capture the absolute value of metabolic rate (Table 1). An ideal model will increase the same as metabolic rate or have a linear estimate as close to one as possible. While all the models reveal a slope that is significantly different than one, the Margaria model (2.04 ± 0.119 [1.92-2.16]; mean ± SEM [95%CI]) and Lichtwark model (0.452 ± 0.0412 [0.411-0.493]) predicted a slope closer to one than other models. This may indicate that the Margaria and Lichtwark may have the best absolute prediction of the changes in metabolic rate. The Bhargava, Uchida, and Umberger models all had slopes significantly higher, under-predicting the absolute change of the metabolic rate.

We completed a similar analysis using repeated-measures correlation (RMCORR) and found that the results still hold with Margaria having the best prediction ($R^2 = 0.846$, Tab. 2). Most of the other metabolic representations were fairly similar (Uchida $R^2 = 0.836$, Bhargava $R^2 = 0.821$, Umberger $R^2 = 0.805$), with the Lichtwark model still lagging behind ($R^2 = 0.712$). The same trend for the slope of the linear estimate is very similar to the previous analysis, with the Margaria (slope = 1.97) and Licthwark (slope = 0.481) being most similar to one.

The relation between effort models and metabolic rate

Many of the neuromechanical effort representations performed poorly compared to the metabolic representations, though some were comparable and better (Fig. 4). A common estimate used in computational motor control, sum of joint torques rate squared, performed poorly compared to the metabolic representations ($R^2 = 0.489$). Joint work and joint work rate performed very well in terms of R^2 value when compared to metabolic rate with R^2 equal to 0.596 and 0.638 respectively. Torque rate performed comparably to the metabolic estimates with an R^2 of 0.536. Similar findings were obtained using a repeated-measures correlation. Work and work rate provided the highest RMCORR coefficient of 0.832 and 0.857 respectively.

Representation	R^2 [LB-UB]	Slope [LB-UB]	Slope SE
Margaria	0.61466 [0.52988 - 0.69944]	2.0412 [1.9227 - 2.1597]	0.11851
Uchida	0.59909 [0.51202 - 0.68617]	2.8647 [2.6929 - 3.0365]	0.17183
Bhargava	0.56738 [0.47593 - 0.65883]	3.4938 [3.2701 - 3.7175]	0.2237
Umberger	0.5427 [0.44817 - 0.63724]	3.9166 [3.653 - 4.1802]	0.26362
Lichtwark	0.39304 [0.28626 - 0.49983]	0.45207 [0.41088 - 0.49326]	0.041192
Torque	0.48094 [0.37992 - 0.58195]	17.169 [15.861 - 18.477]	1.3079
$Torque^2$	0.46182 [0.35918 - 0.56445]	2.7912 [2.5703 - 3.0121]	0.22093
Torque Rate	0.53599 [0.44066 - 0.63132]	1.4651 [1.3652 - 1.5651]	0.099955
Torque $Rate^2$	0.48978 [0.38958 - 0.58998]	0.038847 [0.03594 - 0.041754]	0.0029072
Work	0.59616 [0.50865 - 0.68366]	21.394 [20.103 - 22.685]	1.2911
$Work^2$	0.50255 [0.40358 - 0.60151]	4.3141 [3.9994 - 4.6288]	0.31472
Work Rate	0.63791 [0.55676 - 0.71907]	2.6279 [2.4827 - 2.7731]	0.14517
Work $Rate^2$	0.50865 [0.41031 - 0.60699]	0.060783 [0.056402 - 0.065163]	0.0043804
Muscle Force	0.4919 [0.3919 - 0.5919]	0.013082 [0.012107 - 0.014057]	0.00097489
Muscle $Force^2$	0.45912 [0.35628 - 0.56197]	0.00015415 [0.00014188 - 0.00016642]	1.23E-05
Active State	0.41375 [0.30793 - 0.51957]	166.82 [152.26 - 181.38]	14.56
Active $State^2$	0.40199 [0.29559 - 0.50839]	569.12 [518.22 - 620.02]	50.897
Neural $Drive^2$	0.45737 [0.35439 - 0.56035]	642.73 [591.39 - 694.06]	51.332
Neural $Drive^2$	0.50102 [0.4019 - 0.60013]	664.86 [616.21 - 713.51]	48.651

Table 1. Linear model attributed for each representation. Columns are R^2 values with lower (LB) and upper bound (UB) on R^2 estimate, the linear estimate, lower (LB) and upper bounds (UB) on linear estimate, and the standard error of the slope (SE).

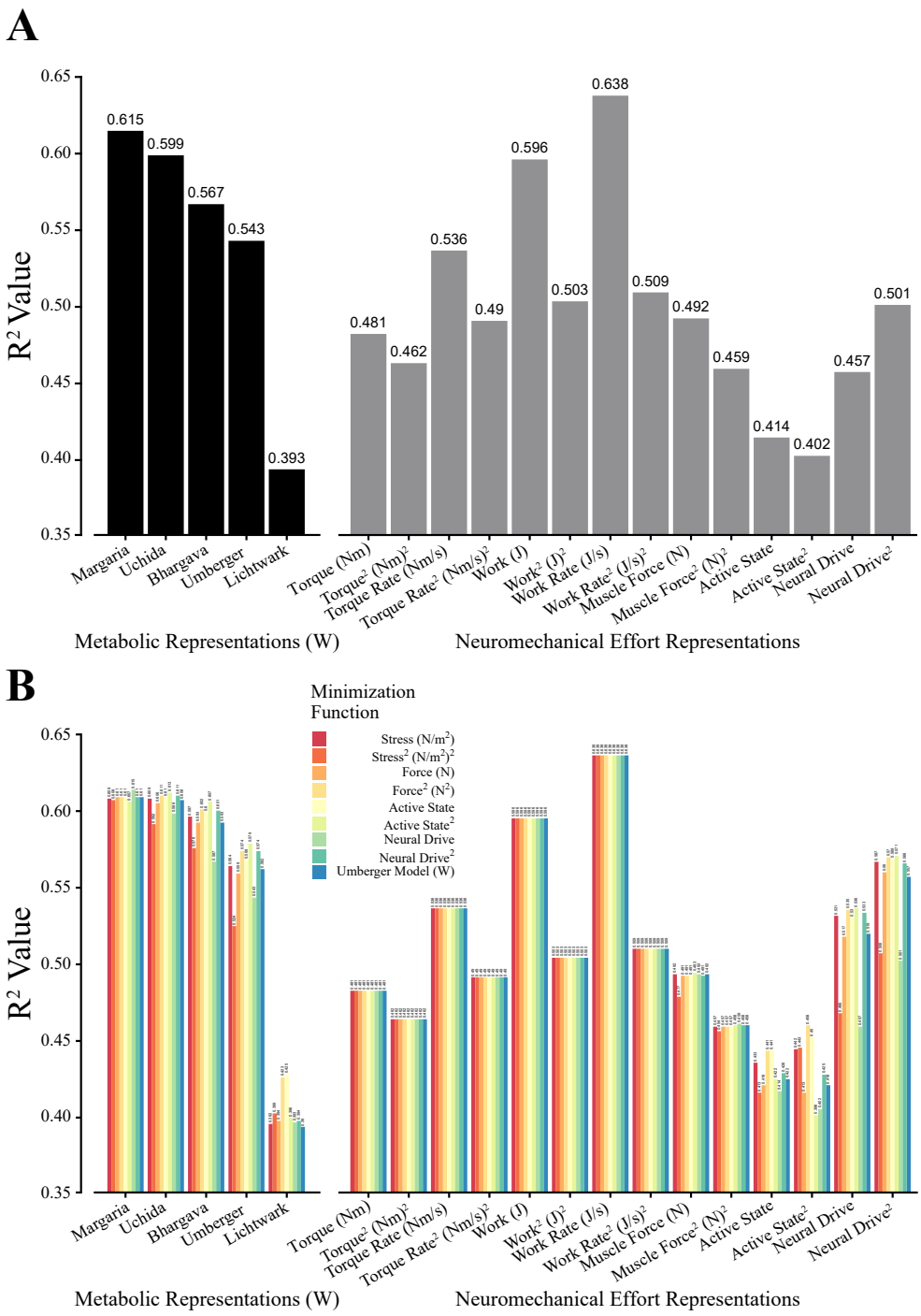

Fig 2. Correlation coefficients of representation predicting metabolic rate. In both plots the x axis is representation, with metabolic representations on the left and neuromechanical effort representations on the right. A. Computed R^2 values for the best fit minimizing neural drive. B. R^2 value as a function of the minimization parameter and the predictor variable for a linear fit. Each bar is a different minimization function, and each grouping is a different metabolic or neuromechanical effort representation.

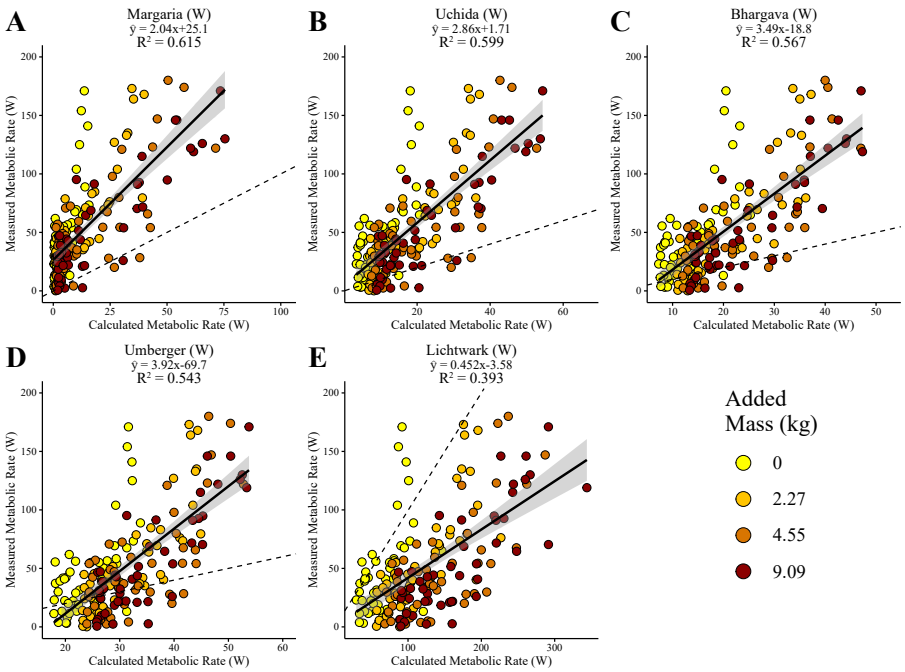

Fig 3. Linear model fits between the metabolic representations and the collected metabolic rate data. In each panel the solid line represents the linear model, and the shaded region shows the standard error bounds of the linear model, and the dashed line represents the line of unity. Each data point represents a metabolic data point (1 subject, 1 mass, 1 speed) and the estimated value from the model colored by mass added at the hand. One data point (movement duration = .54, net metabolic rate = 295) is removed from this figure to improve visualization, but it is not removed for any linear models or analyses. A. The Margaria 1968 model [40]. B. The Uchida 2016 model [23]. C. The Bhargava 2004 model [21]. D. The Umberger 2010 model [19]. E. The Lichtwark 2005 model [24].

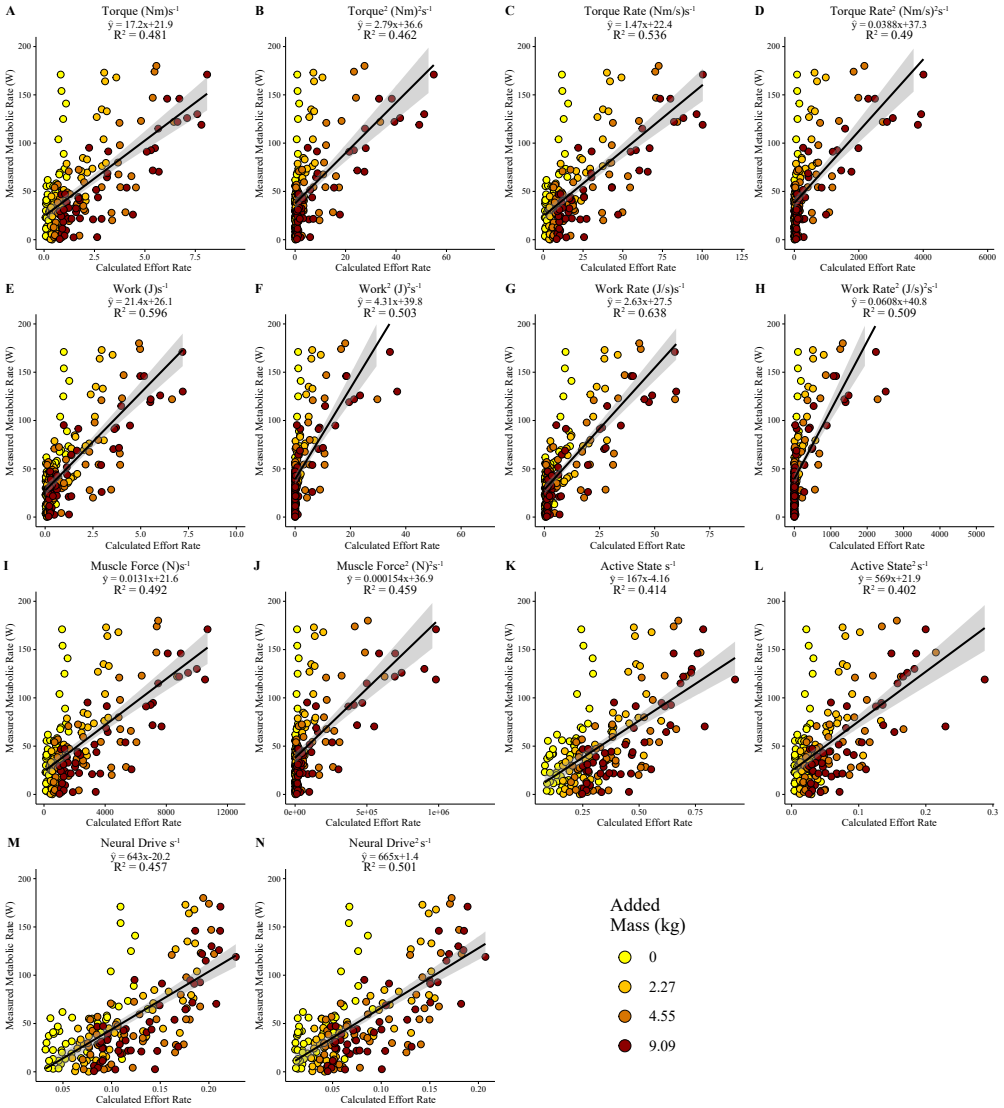

Fig 4. The linear model fits for the four neuromechanical variables and their squared counterparts when minimizing active state squared. In each panel the solid line represents the linear model and the shaded region shows the standard error bounds of the linear model. The data points are colored by mass added at the hand. Panel A, B shows torque and torque squared. C, D torque rate and torque rate squared. E, F show absolute joint work and work squared. G, H show absolute joint work rate and work rate squared. I, J muscle force and muscle force squared. K, L muscle active state and muscle active state squared. M, N neural drive and neural drive squared.

Representation	RMCorr-R^2 [LB-UB]	RMCorr-R^2-Slope
Margaria	0.8457 [0.79801 - 0.88286]	1.9722
Uchida	0.83597 [0.78562 - 0.87531]	2.7757
Bhargava	0.82064 [0.76618 - 0.86339]	3.4445
Umberger	0.80483 [0.74625 - 0.85104]	3.8508
Lichtwark	0.71836 [0.63902 - 0.78258]	0.48056
Torque	0.75086 [0.67896 - 0.80849]	16.635
Torque^2	0.73333 [0.65736 - 0.79454]	2.6971
Torque Rate	0.79074 [0.72857 - 0.83999]	1.4172
Torque Rate^2	0.75485 [0.68389 - 0.81166]	0.037559
Work	0.83231 [0.78097 - 0.87247]	20.649
Work^2	0.75794 [0.68772 - 0.81411]	4.1481
Work Rate	0.85743 [0.813 - 0.89193]	2.5293
Work Rate^2	0.75925 [0.68934 - 0.81515]	0.0583
Muscle Force	0.75924 [0.68933 - 0.81514]	0.012681
Muscle Force^2	0.73237 [0.65619 - 0.79378]	0.00014933
Active State	0.71927 [0.64013 - 0.78331]	170.89
Active State^2	0.73014 [0.65344 - 0.79199]	608.81
Neural Drive^2	0.74163 [0.66757 - 0.80116]	639.74
Neural Drive^2	0.77232 [0.70557 - 0.82548]	657.55

Table 2. Repeated measures correlation attributes for reach representations. Columns are repeated measures correlation R^2, repeated measures correlation R^2 lower (LB) and upper bounds (UB), and repeated measures correlation linear estimate.

Our primary investigation was designed to inform us how single effort representations can estimate experimental metabolic power. The metabolic representations integrate many of these neuromechanical effort representations to create a better prediction of metabolic rate. We can compute a linear model with multiple effort representations to see if combinations of effort can produce reasonable estimates of metabolic power. A linear model with all possible effort representations (torque, torque rate, work, work rate, muscle force, active state, neural drive) was computed using the caret package in R. Doing this we do achieve a higher R^2 (adjusted) value as expected of 0.7288, significantly higher than any other combination. We find that most predictors are significant, with only torque and muscle force as non-significant predictors. This may indicate that a composite cost function should be used as an estimate of metabolic cost, rather than an individual effort representation [8].

Comparing metabolic and predicted estimate distributions

We also compared the approximate distributions of all the representations to metabolic rate as an alternative to R^2. Figure 5 shows these results for all the metabolic models and specific neuromechanical effort models. The estimated distributions are shown in figure 5A and the difference from the metabolic distribution in figure 5B. We found that, of the metabolic models, the Margaria and Uchida models had the lowest integrated density difference compared to the metabolic rate data (Fig. 5C). Of the neuromechanical effort models, torque rate, work, work rate, and active state squared showed similar KDF differences as the Margaria and Uchida models. The Margaria model had the highest p-value in the KS test showing that the Margaria model distribution may be the most similar to the metabolic data, although the test did indicate the Margaria distribution was significantly different than the experimental metabolic distribution (Fig. 5D). This analysis provides another metric, other than R-squared, that indicates that the Margaria model is the best predictor of

experimentally collected metabolic rate out of the metabolic representations.

Effect of mass and speed on metabolic and effort representations

In addition to investigating the variance accounted for by the metabolic and neuromechanical effort representations, we can compare how the measured metabolic rate and each candidate representation vary with mass and movement duration. For example, a measure may have weak explanatory power as evidenced by the R^2 value, but it may nonetheless accurately capture how metabolic rate varies with mass or duration. For a representation to be a good fit, we would expect it to scale in the same manner as metabolic power. To determine this, we parameterized metabolic power and each metabolic and effort representation, as a function of mass and movement duration (Eq. 4. Results are shown for the scaling of mass and time in figure 6 and all parameters are listed in table 3).

When fit to the measured metabolic data, eq. 4, we obtained the following parameters (all of which are significantly different than 0): a = 23.7±2.91 [18.01-29.43], b = 1.05±0.476 [0.0012-0.0198], c = 0.793±9.007e-2 [0.616-0.969], d = 5.634±0.5451 [4.566-6.702] (mean ± standard error [95% confidence interval], Tab. 3). For the ensuing analysis, we will focus specifically on parameters a, c and d. The parameter b represents a scaling factor applied to each representation and is not important for this analysis.

The parameter a in this equation represents the metabolic offset. In theory its existence suggests that a zero-velocity movement still incurs a metabolic rate which has been shown previously for both reaching and walking metabolics [6, 49]. For the Uchida, Bhargava, and Umberger metabolic calculations the fitted a parameter is similarly statistically greater than 0 (Uchida = 2.41±0.615 [2.34-3.61], Bhargava: a = 4.35±1.02 [2.34-6.35], Umberger: a = 14.2±1.23 [11.8-16.6]). None of the neuromechanical effort representations produce an offset that is significantly greater than zero.

The parameter c captures how metabolic rate is affected by the mass being moved (Fig. 6A). Like the metabolic rate data, the scaling of mass, c, is significantly less than one for all metabolic representations except Margaria. However, only the Uchida (c = 0.813±0.0301 [7.54-0.872], Bhargava (c = 0.624±0.0379 [0.55-0.699]), and Lichtwark model (c = 0.588±0.0619 [0.467-0.710]) scale with mass in a manner not significantly different than that observed in the measured metabolic rate data. Most of the neuromechanical representations scaled with mass to a power greater than one except for active state (c = 0.603±0.0524 [0.501-0.706]). Notably, sum of torque squared and muscle force squared significantly overestimate the cost of added mass.

How the representations and metabolic rate are affected by movement duration is represented by the parameter d (Fig. 6B). Metabolic power scales with time by an exponent of 5.6 (d = 5.634±0.5451 [4.566-6.702]), whereas many of the other candidate representations are around the range of 2.5. The Margaria model, with the highest scaling (d = 4.12±0.137 [3.85-4.38]) is closest at capturing this effect of time. However, none of the metabolic representations were statistically similar to metabolic power. Interestingly, sum of torque squared (d = 5.08±0.167 [4.76-5.41]), sum of torque rate squared (d = 6.41±0.203 [6.01-6.81]), sum of work rate (d = 4.93±0.173 [4.59-5.27]), and sum of muscle force squared (d = 5.11±0.179 [4.76-5.46]) were the only neuromechanical effort representation that scaled with movement duration similarly to metabolic power. This means that generally, at the very fast speeds (low movement durations), the representations are all under-predicting the cost of the movement. Work and work rate (squared) also have high d parameters, which may be aiding these fits when predicting metabolic power. The scaling with time exemplifies one of the primary faults of the metabolic representations; they generally cannot account for the sharp rise in metabolic power in the low mass high speed conditions.

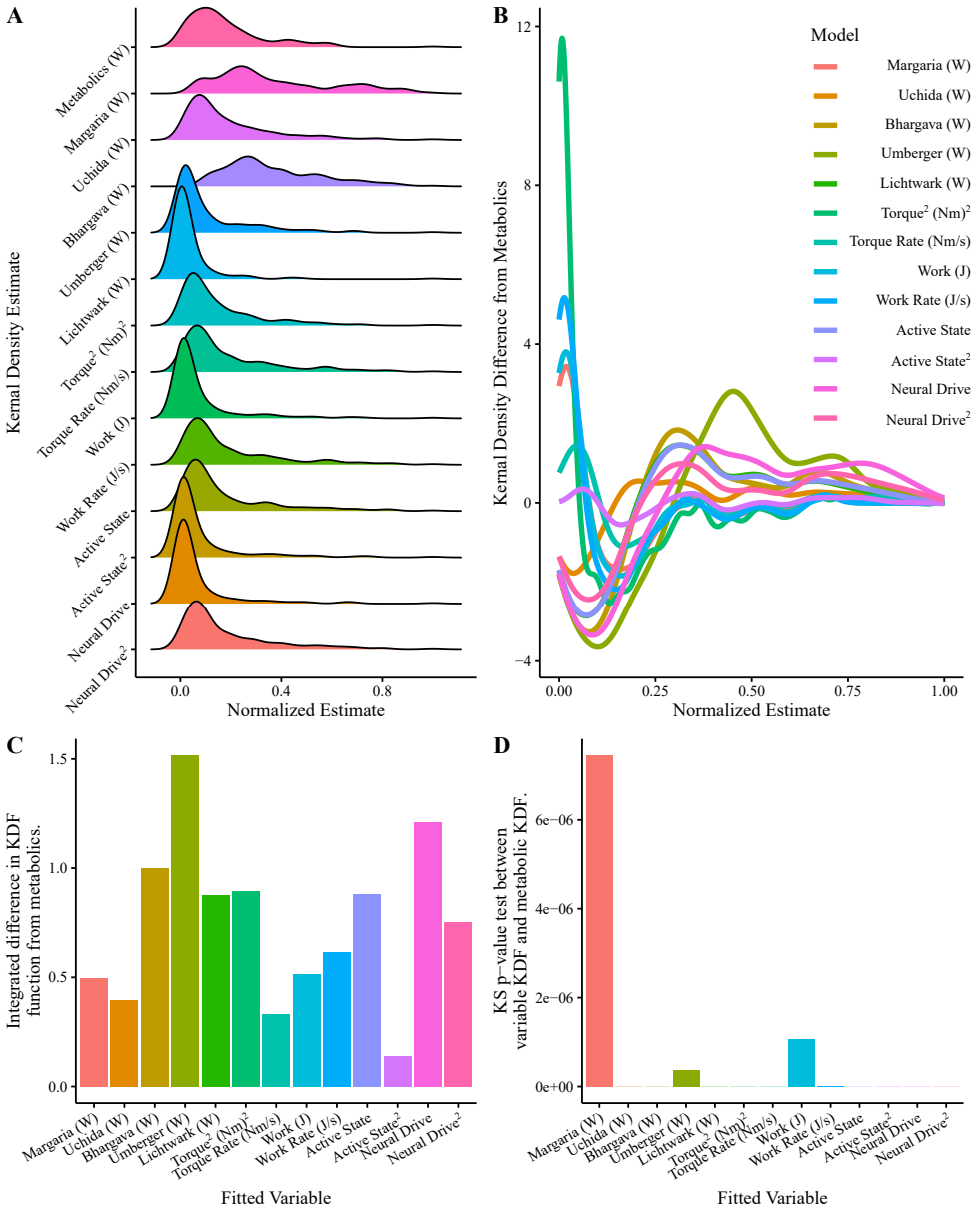

Fig 5. A. Kernal Density Functions (KDF) for specfic metabolic and nueromechanical representations. B. Difference in density distribution from metabolic power. This is calculated as representation minus experimental density. C. Summed (integrated) difference in KDF from representation to experimental metabolics. We find that sum of torque and the Uchida model had the lowest total integrated difference in densities when compared to experimental metabolics. D. Kolmogorov–Smirnov test p-values. The Margaria model showed the most similarity to the experimental metabolic power distribution, but is still significantly different.

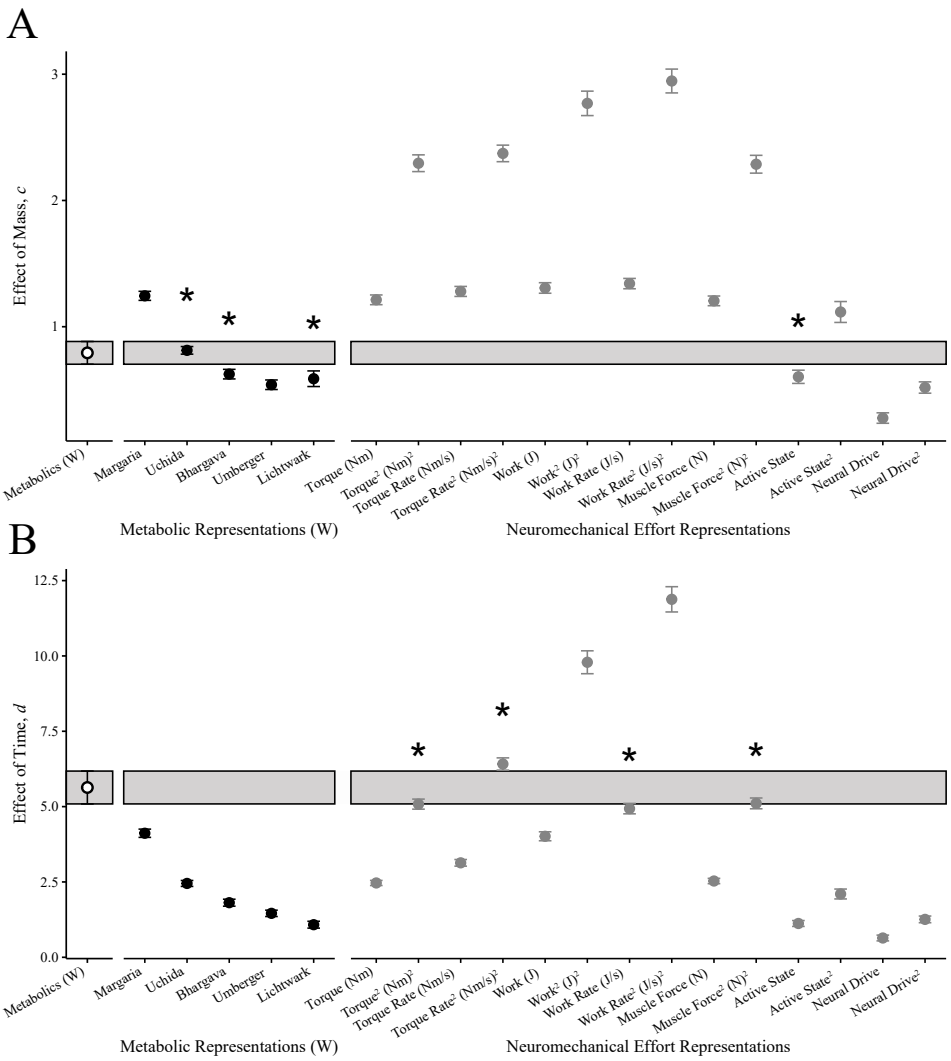

Fig 6. Parameterization values for each representation. Each Value shown mean ± standard error. In this plot we show the scaling of mass, c, and time, d for each representation. If the parameterized value is not different than the parameter from metabolic rate as determined by equation 5, it is indicated with a *.

Representation	a	b
Metabolics	23.7 ± 2.91 (18.01-29.43)	1.05 ± 0.476 (0.0012-0.0198)
Margaria	-0.31 ± 0.471 (-1.23-0.613)	0.416 ± 0.0589 (0.3-0.531)
Uchida	2.41 ± 0.615 (1.2-3.61) *	1.97 ± 0.239 (1.51-2.44)
Bhargava	4.35 ± 1.02 (2.34-6.35) *	3.58 ± 0.574 (2.46-4.71)
Umberger	14.2 ± 1.23 (11.8-16.6) *	4.87 ± 0.801 (3.3-6.44)
Lichtwark	-17.5 ± 15.2 (-47.3-12.3)	40.5 ± 9.88 (21.1-59.9)
Torque	-0.162 ± 0.0705 (-0.3–0.0235)	0.114 ± 0.0148 (0.0848-0.143)
Torque^2	-0.125 ± 0.238 (-0.592-0.341)	0.0133 ± 0.00286 (0.00774-0.0189)
Torque Rate	0.0284 ± 0.754 (-1.45-1.51)	0.842 ± 0.118 (0.61-1.07)
Torque Rate^2	6.89 ± 16.4 (-25.2- 39)	0.414 ± 0.0944 (0.229-0.599)
Joint Work	-0.043 ± 0.0493 (-0.14-0.0537)	0.0356 ± 0.0057 (0.0244-0.0468)
Joint Work^2	0.264 ± 0.184 (-0.0975-0.625)	0.000242 ± 9.19e-05 (6.19e-05-0.000422)
Work Rate	-0.0372 ± 0.357 (-0.737-0.663)	0.169 ± 0.0285 (0.114-0.225)
Work Rate^2	20.4 ± 12.5 (-4.08-44.9)	0.00366 ± 0.00147 (0.000775-0.00654)
Muscle Force	-185 ± 93.1 (-367–2.53)	149 ± 19.5 (111- 187)
Muscle Force^2	-3.48e+03 ± 4.58e+03 (-1.25e+04-5.5e+03)	242 ± 55.3 (133- 350)
Active State	-0.0473 ± 0.0343 (-0.115-0.0199)	0.107 ± 0.0218 (0.0639-0.15)
Active State^2	-0.00379 ± 0.00475 (-0.0131-0.00551)	0.00458 ± 0.00127 (0.00209-0.00707)
Neural Drive	-0.0913 ± 0.0306 (-0.151–0.0313)	0.113 ± 0.0273 (0.0599-0.167)
Neural Drive^2	-0.03 ± 0.00948 (-0.0486–0.0114)	0.0335 ± 0.00648 (0.0208-0.0462)

Representation	c	d
Metabolics	0.793 ± 9.007e-2 (0.616-0.969)	5.634 ± 0.5451 (4.566-6.702)
Margaria	1.24 ± 0.0358 (1.17-1.31)	4.12 ± 0.137 (3.85-4.38)
Uchida	0.813 ± 0.0301 (0.754-0.872) †	2.45 ± 0.0988 (2.26-2.64)
Bhargava	0.624 ± 0.0379 (0.55-0.699) †	1.81 ± 0.116 (1.58-2.04)
Umberger	0.54 ± 0.0378 (0.466-0.615)	1.46 ± 0.105 (1.25-1.66)
Lichtwark	0.588 ± 0.0619 (0.467-0.71) †	1.08 ± 0.114 (0.858- 1.3)
Torque	1.21 ± 0.0385 (1.14-1.29)	2.47 ± 0.0848 (2.3-2.63)
Torque^2	2.29 ± 0.0664 (2.16-2.42)	5.08 ± 0.167 (4.76-5.41)†
Torque Rate	1.28 ± 0.0396 (1.2-1.36)	3.13 ± 0.11 (2.92-3.35)
Torque Rate^2	2.37 ± 0.0655 (2.24- 2.5)	6.41 ± 0.203 (6.01-6.81) †
Joint Work	1.31 ± 0.0417 (1.23-1.39)	4.02 ± 0.149 (3.72-4.31)
Joint Work^2	2.77 ± 0.0968 (2.58-2.96)	9.79 ± 0.38 (9.05-10.5)
Work Rate	1.34 ± 0.0409 (1.26-1.42)	4.93 ± 0.173 (4.59-5.27) †
Work Rate^2	2.95 ± 0.0944 (2.76-3.13)	11.9 ± 0.419 (11.1-12.7)
Muscle Force	1.2 ± 0.0383 (1.13-1.28)	2.53 ± 0.0878 (2.36- 2.7)
Muscle Force^2	2.29 ± 0.0706 (2.15-2.43)	5.11 ± 0.179 (4.76-5.46) †
Active State	0.603 ± 0.0524 (0.501-0.706) †	1.12 ± 0.0977 (0.93-1.31)
Active State^2	1.12 ± 0.0828 (0.954-1.28)	2.1 ± 0.164 (1.78-2.42)
Neural Drive	0.277 ± 0.0414 (0.195-0.358)	0.64 ± 0.0955 (0.453-0.827)
Neural Drive^2	0.518 ± 0.0448 (0.431-0.606)	1.26 ± 0.111 (1.04-1.47)

Table 3. Parameterization values for each representation. Each value shown mean ± standard error with the 95% confidence interval in parenthesis. The a parameter represents some offset at infinite movement duration, for this analysis a value greater than 0 is indicated with a *. A scaling parameter, b, is not important to this analysis. How each representation scales with mass, c, and how they are affected by time, d, are tested to determine if they are different than the parameters found in the metabolic rate with equation 5. This non-difference from metabolic rate effect of mass or time is indicated with a †.

Conclusion

The goal of this study was to determine how well different metabolic and neuromechanical effort representations are able to capture the metabolic rate of arm reaching movements. We collected metabolic data from subjects making reaching movements at a range of speeds and masses added at the hand. We developed a neuromechanical model of the arm and computed model-based representations for metabolic rate and effort and compared these to measured metabolic rate of arm reaching. We found that nearly all the metabolic representations performed well in predicting metabolic rate, with the Margaria energy expenditure model able to provide the best predictive performance. Metabolic models also capture the near-linear scaling of metabolic rate with added mass, as well as the non-zero cost of a movement of infinite duration. In contrast, most of the neuromechanical effort measures performed poorly in comparison, overestimate the cost of added mass, and do not predict a cost for a movement of infinite duration.

We found that the Margaria metabolic model provided the best estimate of the metabolic power of reaching, with most of the other metabolic representations performing similarly, albeit somewhat worse. In theory, these metabolic representations which have been validated in walking should perform similarly in reaching as they are based on general muscle properties. A recent study validated multiple metabolic models in a walking simulation and found relatively similar results [18]. Koelewijn et al. however, found that the Bhargava model predicted the highest R^2 value [21] while in our analysis, out of the metabolic representations the Margaria model performed the best. While the Koelewijn study reports correlation coefficients above 0.9, (seemingly much greater that the R^2 values we report), they used a repeated measures correlation. As a secondary analysis we performed a repeated measures correlation and obtained similar findings regarding the relative performance of each model, but with the correlation coefficients obtained being higher. Specifically, we obtained a correlation coefficient of 0.846 (0.798 - 0.882) for the Margaria model, similar to the 0.90 (0.84 - 0.94) obtained for the Margaria model for walking data. In this study all metabolic representations but the Lichtwark model underpredicted the metabolic rate similar to Koelewijn et al.

When simulating arm reaching movements many different neuromechanical effort costs have been proposed to represent the effort cost of reaching [8, 39, 17, 20]. While these effort representations can capture the general shape of the metabolic rate of reaching, we show that in certain situations these representations may not be good to use to estimate metabolic rate. A common representation of cost in arm reaching, sum of squared joint torques, performs poorly when predicting metabolic rate with an R^2 of 0.462 (0.359 – 0.564). Similar to squared joint torque, squared torque rate also does poorly ($R^2 = 0.489$ [0.390-0.590]). Many of the other neuromechanical representations show similarly low R^2 values. Many of these representations fail at specific aspects of the changing cost landscape, either scaling far too much with mass or scaling far too little with time. Interestingly, joint work ($R^2 = 0.596$ [0.509-0.684]) and joint work rate ($R^2 = 0.634$ [0.557-0.719]) performed significantly better than the other neuromechanical representations. We show that using specific neuromechanical representations of metabolic rate may lead to inaccurate results as these representations do not well represent metabolic rate.

We can also compare how each of these representations exhibit an offset to the cost of movement as well as how they change with mass and speed. Ideally, the representation will exhibit an offset to the cost of movement and scale to the same degree as metabolic rate with either mass or speed. The offset parameter (a) represents the metabolic rate of a reach of infinite duration. The metabolic rate data revealed an offset value significantly greater that zero, indicative of a cost that is independent of mass and time. The Umberger, Bhargava, and Uchida model have an offset greater than

0. The offset value fitted via the Umberger model was the most similar to the metabolic rate data fit. All of the neuromechanical representations lack an offset that is greater than 0, implying that as the movement duration increases to infinity, joint torque, joint work, muscle force, active state, and neural drive will all, not surprisingly, asymptote to 0. Thus, a major limitation of these neuromechanical representations is that they cannot account for this offset which may lead to more inaccurate predictions.

We also focus on how these representations change with mass and time. Metabolic power was increased by mass (c) to the power of 0.793, a slightly sub-linear scaling. The sub-linear increase in metabolic power due to mass was captured by all metabolic representations but the Margaria model. The Uchida (0.813±0.0301 [0.754-0.872]), Bhargava (0.624±0.0379 [0.550-0.699]), and Lichtwark (0.588±0.0619 [0.467-0.710]) model were also not significantly different than the scaling of mass of the metabolic rate data. Almost all the neuromechanical effort representations (except active state) scaled supra-linearly with mass, likely leading to a large source of error in these estimates. The very sharp rise in metabolic power due to an increase in speed is very super-linear with an exponent of of 5.6 (d = 5.634±0.5451 [4.566-6.702]), but none of the metabolic representations reflect a similar sharp rise, as evidenced by how they scale with movement duration and quantified by the fitted d parameter. Margaria was the closest at 4.12 (d = 4.12±0.137 [3.85-4.38]), but is still much lower than the metabolic data. This may lead to large sources of error with the metabolic representations, as they seem unable to account for the sharp rise in metabolic rate at very fast speeds.

There may be many possible explanations as to why the low mass very fast movements seem to be generally under predicted by the models. One possible explanation is that for the very fast movements, although not much force is being generated the rapid onset of muscle activation and rapid decay may not be as costly as required in the metabolic representations. Increasing the cost to send a signal to muscles may address some of the issues with modeling low mass movements. By applying machine learning methods one may be able to optimize the parameters within a metabolic representation to better represent the collected metabolic rate.

It is unclear which minimization function humans use to determine which muscles get activated versus others. Some evidence points towards minimizing the activation state of the muscle activation and effort [16, 50, 51, 52, 53, 54]. Because of this, we computed the metabolic and effort estimates while utilizing many possible minimization functions. We found that minimizing neural drive led to the highest R^2 value, which is presented in the main body results. Previous work has shown that when compared to EMG muscle activation, minimizing active state squared provides a good representation of how the muscles are activated [16]. Minimizing active state squared, like previous work, predicts the highest R^2 for some representations (Uchida, Bhargava, Umberger) but did not for Margaria. In general, our results do not change significantly with changing minimization function (Fig. 2B). However, for some of these metabolic and effort representations, the minimization function had a large effect on the predictive power. The representation of neural drive for example, had a maximum R^2 value of 0.536 minimizing active state squared. When minimizing neural drive, neural drive dropped in predictive power to 0.457. Interestingly, minimizing neural drive had relatively low predictive power across all representations. Since some data aligns with the theory that minimizing active state squared yields the best prediction of muscle force, active state squared may be the best objective function to use with more recent metabolic representations.

The calculation of metabolic rate can be calculated in multiple ways and leads metabolic rate estimates being fairly noisy. This is more evident at the higher movement duration lower cost movements. Metabolic rate noisiness may be contributing significantly to errors in the metabolic prediction of the neuro-mechanical model. Other possible equations exist to calculate metabolic energy and it has been suggested other

equations may provide better estimates of metabolic rate in specific circumstances [55]. Kipp et al. indicate that the Peronnet equation may have a better estimation of metabolic rate because Peronnet does not treat O_2 and CO_2 as ideal gasses [55, 56]. The Brockway and Peronnet equation do not calculate significantly different metabolic rates and thus we followed previous work and used the Brockway equation.

We did not collect EMG data in this current study and thus we cannot determine specifically which minimization function was being utilized by our subjects. Using the EMG data we may have been able to compute a better estimate for metabolic rate and more accurate muscle forces [57]. Co-contraction may have contributed significantly to the metabolic rate at the faster speeds or higher masses at the beginning of the movement. However, our model is not able to account for co-contraction at the onset of the movement and an EMG analysis may have aided this. The way our model may be able to show co-activation is simultaneous activation of opposing muscles through either active state or neural drive. Within the reaching movement our model does predict some co-contraction (active state and neural drive) as the arm needs to slow down the movement to hit the target, but the primary source of co-contraction would be primarily at the beginning of the movement which we cannot account for.

This analysis shows that current models of metabolic expenditure used for explaining walking metabolics are also able to generally predict reaching metabolics as well, with the Margaria model providing the best predictive power and the Uchida model in close second. Of the neuromechanical effort representations, only torque rate, work, and work rate showed a good relation to metabolic power, and sometimes better predictions than metabolic representations. Critically, sum of squared joint torque, an oft-used measure of effort in computational models was found to be a substantially less accurate predictor of the metabolic cost of reaching.

Supporting information

S1 File Neuromechanical model. Description of the neuromehcanical arm model used in this study. This document describes the process of using kinematic data to simulate arm reaches.

S2 File Metabolic rate models. Description of the metabolic rate models simulated in this study.

References

1. T Flash and N Hogan. The coordination of arm movements: an experimentally confirmed mathematical model. *Journal of Neuroscience*, 5(7):1688–1703, jul 1985.

2. Jessica C Selinger, Shawn M O'Connor, Jeremy D Wong, and J Maxwell Donelan. Humans Can Continuously Optimize Energetic Cost during Walking. *Current Biology*, 25(18):2452–2456, sep 2015.

3. R McN. Alexander. A minimum energy cost hypothesis for human arm trajectories. *Biological Cybernetics*, 76(2):97–105, feb 1997.

4. Richard P Heitz. The speed-accuracy tradeoff: history, physiology, methodology, and behavior. *Frontiers in Neuroscience*, 8, 2014.

5. J Maxwell Donelan, Rodger Kram, and Arthur D Kuo. Mechanical work for step-to-step transitions is a major determinant of the metabolic cost of human walking. *Journal of Experimental Biology*, 205(23):3717–3727, dec 2002.

6. Reza Shadmehr, Helen J. Huang, and Alaa A. Ahmed. A Representation of Effort in Decision-Making and Motor Control. *Current Biology*, 26(14):1929–1934, jul 2016.

7. H J Ralston. Energy-speed relation and optimal speed during level walking. *Internationale Zeitschrift für angewandte Physiologie einschließlich Arbeitsphysiologie*, 17(4):277–283, oct 1958.

8. Bastien Berret, Enrico Chiovetto, Francesco Nori, and Thierry Pozzo. Evidence for composite cost functions in arm movement planning: An inverse optimal control approach. *PLoS Computational Biology*, 7(10):e1002183, oct 2011.

9. Natalia Sánchez, Sungwoo Park, and James M Finley. Evidence of Energetic Optimization during Adaptation Differs for Metabolic, Mechanical, and Perceptual Estimates of Energetic Cost. *Scientific Reports*, 7(1):7682, aug 2017.

10. Timothy M Griffin, Thomas J Roberts, and Rodger Kram. Metabolic cost of generating muscular force in human walking: insights from load-carrying and speed experiments. *Journal of Applied Physiology*, 95(1):172–183, jul 2003.

11. Keith E Gordon, Daniel P Ferris, and Arthur D Kuo. Metabolic and Mechanical Energy Costs of Reducing Vertical Center of Mass Movement During Gait. *Archives of Physical Medicine and Rehabilitation*, 90(1):136–144, jan 2009.

12. Ross H Miller, Brian R Umberger, Joseph Hamill, and Graham E Caldwell. Evaluation of the minimum energy hypothesis and other potential optimality criteria for human running. *Proceedings of the Royal Society of London B: Biological Sciences*, page rspb20112015, nov 2011.

13. Ross H Miller. A comparison of muscle energy models for simulating human walking in three dimensions. *Journal of Biomechanics*, 47(6):1373–1381, apr 2014.

14. Helen J Huang, Rodger Kram, and Alaa A Ahmed. Reduction of Metabolic Cost during Motor Learning of Arm Reaching Dynamics. *Journal of Neuroscience*, 32(6):2182–2190, feb 2012.

15. K N An, B M Kwak, E Y Chao, and B F Morrey. Determination of Muscle and Joint Forces: A New Technique to Solve the Indeterminate Problem. *Journal of Biomechanical Engineering*, 106(4):364–367, nov 1984.

16. Andrew H Fagg, Ashvin Shah, and Andrew G Barto. A Computational Model of Muscle Recruitment for Wrist Movements. *Journal of Neurophysiology*, 88(6):3348–3358, dec 2002.

17. W Li and E Todorov. Iterative linearization methods for approximately optimal control and estimation of non-linear stochastic system. *International Journal of Control*, 80(9):1439–1453, sep 2007.

18. Anne D Koelewijn, Dieter Heinrich, and Antonie J van den Bogert. Metabolic cost calculations of gait using musculoskeletal energy models, a comparison study. *bioRxiv*, page 588590, jul 2019.

19. Brian R Umberger. Stance and swing phase costs in human walking. *Journal of The Royal Society Interface*, 7(50):1329–1340, sep 2010.

20. Brian R Umberger, Karin. G M Gerristen, and Philpe. E Martin. A Model of Human Muscle Energy Expenditure. *Computer Methods in Biomechanics and Biomedical Engineering*, 6(2):99–111, may 2003.

21. Lindsay J Bhargava, Marcus G Pandy, and Frank C Anderson. A phenomenological model for estimating metabolic energy consumption in muscle contraction. *Journal of Biomechanics*, 37(1):81–88, jan 2004.

22. A E Minetti and R McN. Alexander. A Theory of Metabolic Costs for Bipedal Gaits. *Journal of Theoretical Biology*, 186(4):467–476, jun 1997.

23. Thomas K Uchida, Jennifer L Hicks, Christopher L Dembia, and Scott L Delp. Stretching Your Energetic Budget: How Tendon Compliance Affects the Metabolic Cost of Running. *PLOS ONE*, 11(3):e0150378, mar 2016.

24. G A Lichtwark and A M Wilson. A modified Hill muscle model that predicts muscle power output and efficiency during sinusoidal length changes. *Journal of Experimental Biology*, 208(15):2831–2843, aug 2005.

25. R Margaria. *On the physiology and especially on the energy consumption of the march and the race at various speeds and inclinations of the ground.* Mem. d. R. accad. naz. dei Lincei, classe di sci. fis., mat. e nat. Bardi, 1938.

26. Joo H Kim and Dustyn Roberts. A joint-space numerical model of metabolic energy expenditure for human multibody dynamic system. *International Journal for Numerical Methods in Biomedical Engineering*, 31(9):e02721, 2015.

27. Y Uno, M Kawato, and R Suzuki. Formation and control of optimal trajectory in human multijoint arm movement. Minimum torque-change model. *Biological Cybernetics*, 61(2):89–101, 1989.

28. Eri Nakano, Hiroshi Imamizu, Rieko Osu, Yoji Uno, Hiroaki Gomi, Toshinori Yoshioka, and Mitsuo Kawato. Quantitative Examinations of Internal Representations for Arm Trajectory Planning: Minimum Commanded Torque Change Model. *Journal of Neurophysiology*, 81(5):2140–2155, may 1999.

29. David Winter. Biomechanics and Motor Control of Human Movement, 4th Edition, oct 2009.

30. Frank C Anderson and Marcus G Pandy. Dynamic Optimization of Human Walking. *Journal of Biomechanical Engineering*, 123(5):381–390, may 2001.

31. Frank C Anderson and Marcus G Pandy. Static and dynamic optimization solutions for gait are practically equivalent. *Journal of Biomechanics*, 34(2):153–161, feb 2001.

32. Herbert Hatze. The fundamental problem of myoskeletal inverse dynamics and its implications. *Journal of Biomechanics*, 35(1):109–115, jan 2002.

33. Boris I Prilutsky and Vladimir M Zatsiorsky. Optimization-Based Models of Muscle Coordination. *Exercise and sport sciences reviews*, 30(1):32, jan 2002.

34. Yoshiaki Taniai and Jun Nishii. Optimality of Upper-Arm Reaching Trajectories Based on the Expected Value of the Metabolic Energy Cost. *Neural Computation*, 27(8):1721–1737, jun 2015.

35. Yu Jiang, Zhong Ping Jiang, and Ning Qian. Optimal control mechanisms in human arm reaching movements. In *Proceedings of the 30th Chinese Control Conference, CCC 2011*, pages 1377–1382, jul 2011.

36. Lelai Zhou, Shaoping Bai, Michael R Hansen, and John Rasmussen. Modeling of Human Arm Energy Expenditure for Predicting Energy Optimal Trajectories. *Modeling, Identification and Control; Kristiansand*, 32(3):91, 2011.

37. Weiguang Si, Sung-Hee Lee, Eftychios Sifakis, and Demetri Terzopoulos. Realistic Biomechanical Simulation and Control of Human Swimming. *ACM Trans. Graph.*, 34(1):10:1—-10:15, dec 2014.

38. Falisse Antoine, Serrancolí Gil, Dembia Christopher L., Gillis Joris, Jonkers Ilse, and De Groote Friedl. Rapid predictive simulations with complex musculoskeletal models suggest that diverse healthy and pathological human gaits can emerge from similar control strategies. *Journal of The Royal Society Interface*, 16(157):20190402, aug 2019.

39. Dinant A Kistemaker, Jeremy D Wong, and Paul L Gribble. The Central Nervous System Does Not Minimize Energy Cost in Arm Movements. *Journal of Neurophysiology*, 104(6):2985–2994, dec 2010.

40. Rodolfo Margaria. Positive and negative work performances and their efficiencies in human locomotion. *Internationale Zeitschrift für angewandte Physiologie einschließlich Arbeitsphysiologie*, 25(4):339–351, dec 1968.

41. J M Brockway. Derivation of formulae used to calculate energy expenditure in man. *Human nutrition : clinical nutrition*, 1987.

42. Renato Contini. Body segment parameters. II. *Artificial limbs*, 16(1):1–19, 1972.

43. I E Brown, E J Cheng, and G E Loeb. Measured and modeled properties of mammalian skeletal muscle. II. The effects of stimulus frequency on force-length and force-velocity relationships. *Journal of Muscle Research and Cell Motility*, 20(7):627–643, oct 1999.

44. Darryl G Thelen. Adjustment of Muscle Mechanics Model Parameters to Simulate Dynamic Contractions in Older Adults. *Journal of Biomechanical Engineering*, 125(1):70, 2003.

45. Jack M Winters. An improved muscle-reflex actuator for use in large-scale neuromusculoskeletal models. *Annals of Biomedical Engineering*, 23(4):359–374, jul 1995.

46. Matthew Millard, Thomas Uchida, Ajay Seth, and Scott L Delp. Flexing Computational Muscle: Modeling and Simulation of Musculotendon Dynamics. *Journal of Biomechanical Engineering*, 135(2):21005–21011, feb 2013.

47. Gervasio Piñeiro, Susana Perelman, Juan Guerschman, and José Paruelo. How to Evaluate Models: Observed vs. Predicted or Predicted vs. Observed? *Ecological Modelling*, 216:316–322, sep 2008.

48. Rory Wolfe and James Hanley. If we're so different, why do we keep overlapping? When 1 plus 1 doesn't make 2. *CMAJ: Canadian Medical Association Journal*, 166(1):65–66, jan 2002.

49. Manoj Srinivasan. Optimal speeds for walking and running, and walking on a moving walkway. *Chaos: An Interdisciplinary Journal of Nonlinear Science*, 19(2):26112, jun 2009.

50. Roy D Crowninshield and Richard A Brand. A physiologically based criterion of muscle force prediction in locomotion. *Journal of Biomechanics*, 14(11):793–801, jan 1981.

51. S L Delp, F C Anderson, A S Arnold, P Loan, A Habib, C T John, E Guendelman, and D G Thelen. OpenSim: Open-Source Software to Create and Analyze Dynamic Simulations of Movement. *IEEE Transactions on Biomedical Engineering*, 54(11):1940–1950, nov 2007.

52. Daniele Borzelli, Denise J Berger, Dinesh K Pai, and Andrea D'Avella. Effort minimization and synergistic muscle recruitment for three-dimensional force generation. *Frontiers in Computational Neuroscience*, 7, dec 2013.

53. Jacek Cholewicki and Stuart M McGill. EMG assisted optimization: A hybrid approach for estimating muscle forces in an indeterminate biomechanical model. *Journal of Biomechanics*, 27(10):1287–1289, oct 1994.

54. J J Collins. The redundant nature of locomotor optimization laws. *Journal of Biomechanics*, 28(3):251–267, mar 1995.

55. Shalaya Kipp, William C Byrnes, and Rodger Kram. Calculating metabolic energy expenditure across a wide range of exercise intensities: the equation matters. *Applied Physiology, Nutrition, and Metabolism*, 43(6):639–642, feb 2018.

56. F Péronnet and D Massicotte. Table of nonprotein respiratory quotient: an update. *Canadian Journal of Sport Sciences = Journal Canadien Des Sciences Du Sport*, 16(1):23–29, mar 1991.

57. Hoa X Hoang, Claudio Pizzolato, Laura E Diamond, and David G Lloyd. Subject-specific calibration of neuromuscular parameters enables neuromusculoskeletal models to estimate physiologically plausible hip joint contact forces in healthy adults. *Journal of Biomechanics*, 80:111–120, 2018.

58. F De Groote, G Pipeleers, I Jonkers, B Demeulenaere, C Patten, J Swevers, and J De Schutter. A physiology based inverse dynamic analysis of human gait: potential and perspectives. *Computer Methods in Biomechanics and Biomedical Engineering*, 12(5):563–574, oct 2009.

59. Ryan Koeppen, Meghan E Huber, Dagmar Sternad, and Neville Hogan. Controlling Physical Interactions: Humans Do Not Minimize Muscle Effort. *Proceedings of the ASME Dynamic Systems and Control Conference. ASME Dynamic Systems and Control Conference.*, page V001T36A003, oct 2017.

60. Reza Shadmehr. Computational Neurobiology of Reaching and Pointing A Foundation for Motor Learning, 2005.

61. Felix E Zajac and Jack M Winters. Modeling Musculoskeletal Movement Systems: Joint and Body Segmental Dynamics, Musculoskeletal Actuation, and Neuromuscular Control. In Jack M Winters and Savio L-Y. Woo, editors, *Multiple Muscle Systems: Biomechanics and Movement Organization*, pages 121–148. Springer New York, New York, NY, 1990.

62. H Houdijk, M F Bobbert, and A de Haan. Evaluation of a Hill based muscle model for the energy cost and efficiency of muscular contraction. *Journal of Biomechanics*, 39(3):536–543, jan 2006.

63. Rainer Hessmer. *Kinematics for Lynxmotion Robot Arm*. oct 2009.

64. Gordon Robertson, Graham Caldwell, Joseph Hamill, Gary Kamen, and Saunders Whittlesey. *Research Methods in Biomechanics, 2E*. Human Kinetics, sep 2013.

65. S Adewusi, S Rakheja, and P Marcotte. Biomechanical models of the human hand-arm to simulate distributed biodynamic responses for different postures. *International Journal of Industrial Ergonomics*, 42(2):249–260, mar 2012.

66. Roger Enoka. *Neuromechanics of Human Movement*. Human Kinetics, 5th edition, 2002.

67. Kun Hwang, Jin Yi Han, and In Hyuk Chung. Topographical Anatomy of the Anconeus Muscle for Use as a Free Flap. *Journal of Reconstructive Microsurgery*, 20(08):631–636, nov 2004.

68. Joseph Langenderfer, Seth A Jerabek, Vijay B Thangamani, John E Kuhn, and Richard E Hughes. Musculoskeletal parameters of muscles crossing the shoulder and elbow and the effect of sarcomere length sample size on estimation of optimal muscle length. *Clinical Biomechanics*, 19(7):664–670, aug 2004.

69. Katherine R S Holzbaur, Wendy M Murray, and Scott L Delp. A Model of the Upper Extremity for Simulating Musculoskeletal Surgery and Analyzing Neuromuscular Control. *Annals of Biomedical Engineering*, 33(6):829–840, jun 2005.

70. J Fridén, D Albrecht, and R L Lieber. Biomechanical analysis of the brachioradialis as a donor in tendon transfer. *Clinical Orthopaedics and Related Research*, (383):152–161, feb 2001.

71. Wendy M Murray, Thomas S Buchanan, and Scott L Delp. The isometric functional capacity of muscles that cross the elbow. *Journal of Biomechanics*, 33(8):943–952, aug 2000.

72. Katherine R S Holzbaur, Scott L Delp, Garry E Gold, and Wendy M Murray. Moment-generating capacity of upper limb muscles in healthy adults. *Journal of Biomechanics*, 40(11):2442–2449, jan 2007.

73. Yi-Wen Chang, Fong-Chin Su, Hong-Wen Wu, and Kai-Nan An. Optimum length of muscle contraction. *Clinical Biomechanics*, 14(8):537–542, oct 1999.

74. Dinant A Kistemaker, Arthur J (Knoek) Van Soest, and Maarten F Bobbert. A model of open-loop control of equilibrium position and stiffness of the human elbow joint. *Biological Cybernetics*, 96(3):341–350, mar 2007.

75. Pascale Pigeon, L'Hocine Yahia, and Anatol G Feldman. Moment arms and lengths of human upper limb muscles as functions of joint angles. *Journal of Biomechanics*, 29(10):1365–1370, oct 1996.

76. Raja Dahmane, Srdjan Djordjevič, Bostjan Šimunič, and Vojko Valenčič. Spatial fiber type distribution in normal human muscle: Histochemical and tensiomyographical evaluation. *Journal of Biomechanics*, 38(12):2451–2459, dec 2005.

77. M A Johnson, J Polgar, D Weightman, and D Appleton. Data on the distribution of fibre types in thirty-six human muscles: An autopsy study. *Journal of the Neurological Sciences*, 18(1):111–129, jan 1973.

78. R L Lieber and S C Bodine-Fowler. Skeletal muscle mechanics: implications for rehabilitation. *Physical Therapy*, 73(12):844–856, dec 1993.

79. T L Wickiewicz, R R Roy, P L Powell, and V R Edgerton. Muscle architecture of the human lower limb. *Clinical Orthopaedics and Related Research*, 179:275–283, oct 1983.

80. Katherine R S Holzbaur, Wendy M Murray, Garry E Gold, and Scott L Delp. Upper limb muscle volumes in adult subjects. *Journal of Biomechanics*, 40(4):742–749, jan 2007.

81. E J van Zuylen, A van Velzen, and J J Denier van der Gon. A biomechanical model for flexion torques of human arm muscles as a function of elbow angle. *Journal of Biomechanics*, 21(3):183–190, jan 1988.

82. Yifeng Jiang, Tom Van Wouwe, Friedl De Groote, and C Karen Liu. Synthesis of Biologically Realistic Human Motion Using Joint Torque Actuation. *arXiv:1904.13041 [cs]*, apr 2019.

83. Sung-Hee Lee, Eftychios Sifakis, and Demetri Terzopoulos. Comprehensive Biomechanical Modeling and Simulation of the Upper Body. *ACM Trans. Graph.*, 28(4):99:1—-99:17, sep 2009.

84. Yi-Chung Lin, Tim W Dorn, Anthony G Schache, and Marcus G Pandy. Comparison of different methods for estimating muscle forces in human movement. *Proceedings of the Institution of Mechanical Engineers, Part H: Journal of Engineering in Medicine*, 226(2):103–112, feb 2012.

85. B Brenner, L C Yu, L E Greene, E Eisenberg, and M Schoenberg. Ca2+-sensitive cross-bridge dissociation in the presence of magnesium pyrophosphate in skinned rabbit psoas fibers. *Biophysical Journal*, 50(6):1101–1108, dec 1986.

86. George I Zahalak and Shi-Ping Ma. Muscle Activation and Contraction: Constitutive Relations Based Directly on Cross-Bridge Kinetics. *Journal of Biomechanical Engineering*, 112(1):52–62, feb 1990.

87. H Hatze. A myocybernetic control model of skeletal muscle. *Biological Cybernetics*, 25(2):103–119, jun 1977.

88. J M Winters and L Stark. Muscle models: What is gained and what is lost by varying model complexity. *Biological Cybernetics*, 55(6):403–420, mar 1987.

89. Marcelo Epstien and Walter Herzog. *Theoretical Models of Skeletal Muscle: Biological and Mathematical Considerations*. 1998.

90. S L Delp, J P Loan, M G Hoy, F E Zajac, E L Topp, and J M Rosen. An interactive graphics-based model of the lower extremity to study orthopaedic surgical procedures. *IEEE Transactions on Biomedical Engineering*, 37(8):757–767, aug 1990.

91. R Horowits. Passive force generation and titin isoforms in mammalian skeletal muscle. *Biophysical Journal*, 61(2):392–398, feb 1992.

92. Jack M Winters and Lawrence Stark. Estimated mechanical properties of synergistic muscles involved in movements of a variety of human joints. *Journal of Biomechanics*, 21(12):1027–1041, jan 1988.

93. Fang Lou, N A Curtin, and R C Woledge. Contraction with shortening during stimulation or during relaxation: how do the energetic costs compare? *Journal of Muscle Research & Cell Motility*, 19(7):797–802, oct 1998.

94. Marco Linari, R C Woledge, and N A Curtin. Energy storage during stretch of active single fibres from frog skeletal muscle. *The Journal of Physiology*, 548(Pt 2):461–474, apr 2003.

Supporting information for "A validation of metabolic energy models in arm reaching"

The primary goal of this musculoskeletal model is to determine the muscle forces that drive the kinematics of arm reaching kinematic data. This supplemental describes the method we used to match the joints' kinematic profiles by simulating muscles as the actuators to produce the joint torques for motion [51, 58].

S1 Neuromechanical Model

A neuromechanically relevant model of the arm was developed that includes the forearm and upper arm, the shoulder and elbow joint, and 8 physiologically relevant muscles crossing both the shoulder and elbow joint to act as actuators (fig. 1B). Movement trajectories were computed from the average trajectories for each subjects' target, mass, and speed condition from the metabolic data collection. Joint torques were calculated using inverse dynamics. We tested multiple minimization functions to distribute the individual muscle forces as it is unclear how humans coordinate muscle contractions [39, 59, 17]. Next, muscle active state, neural drive, and five models for energy expenditure were calculated.

Seven neuromechanical effort representations (absolute joint torques, absolute joint torque rate, absolute joint work, absolute joint work rate, muscle force, muscle active state, and neural drive), their squared counterparts, and the five metabolic representations were fit in a linear model to the collected metabolic power data to determine the correlation between them. We also compared how the neuromechanical proxies and metabolic representations changed with added mass and changing movement duration to test if they were affected by mass and movement duration in a similar manner to metabolic power.

The final calculation estimates the metabolic rate of each muscle through five different metabolic representations [19, 21, 23, 40, 24]. In all representations but Margaria, these costs are split into a few rate components, the activation and maintenance heat rate (h_{AM}), shortening lengthening heat rate (h_{SL}), and the mechanical work rate ($\dot{w}$) [19, 21, 23, 24]. The Margaria model estimates the energetic rate as a function of concentric power and eccentric power [40].

1. The first step is determining the trajectory from experimentally collecting kinematic data (Kinematic Data, Sec. S1) [1].

2. Inverse kinematics is used to determine the joint positions and velocities (Inverse Kinematics, Sec. S1).

3. Inverse dynamics is used to calculate the joint torque's across the joints (Inverse Dynamics, Sec. S1) [60].

4. Using the position of the joints, a muscle model computes the length and velocities of the muscles (Muscle Moment Arms, Sec. S1, Muscle Lengths, Sec. S1). These lengths and velocities are used to compute active state from muscle properties in step 6.

5. After joint positions, torques, and muscle parameters are determined, a muscle model is implemented at every time step to compute the muscle forces required to produce the motion through matching joint torques and minimizing an objective function (step Int 1, S1) [61]. The objective function has 3 inputs, including the objective function being used in the optimization and two constraints: matching

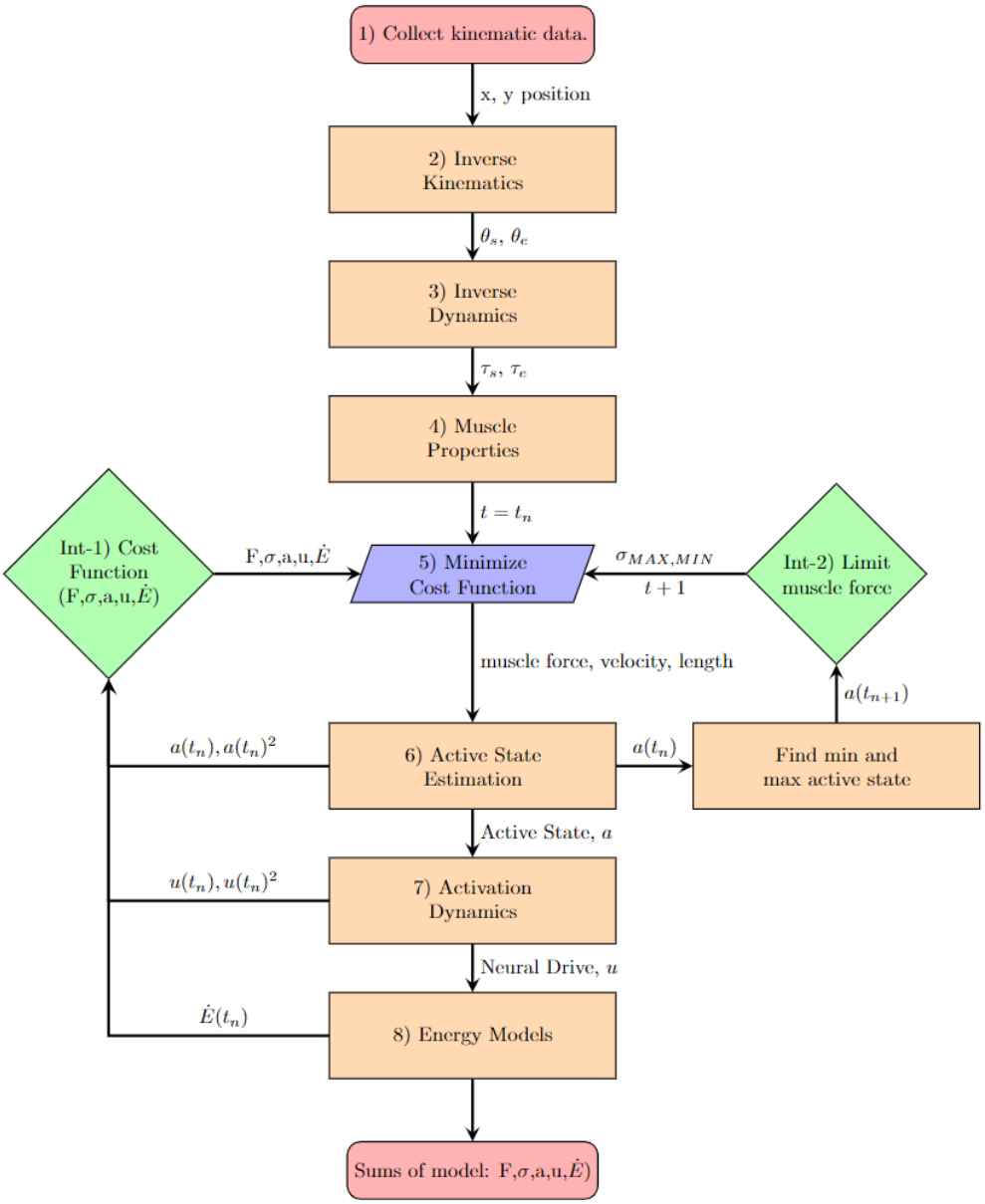

Fig S1. Modeling flow chart for simulating reaching movements.

the torque from the kinematic data and a limit on the change of activation state (Int 2, Sec. S1. The objective function can take many forms including minimizing active state, neural drive, and an energetic model. This is not discussed below as there are many optimization methods that can solve an under-determined system given an objective function.

6. The muscle model takes into account force length and force velocity properties to calculate the active state of the muscle (Active State Estimation, Sec. S1) [43, 46].
7. The control signal is approximated using activation dynamics which generally take the form of first order non-linear filters (Activation Dynamics, Sec. S1) [45, 44, 43, 46].
8. Last, one of many models of metabolic cost can be implemented to simulate the cost of movement (Metabolics Models S1) [20, 19, 23, 21, 40, 62, 24, 22, 22].

Step 1 - Kinematic Data

The biomechanical model was set to make the same reaching movements as in the metabolics data collection. The model simulated reaching movements to and from four different targets located at 45°, 135°, 225°, and 315° from the right horizontal (Figure 1A). This simulated eight targets, with four masses, seven speeds, and eight subjects for a total of 1874. X-Y positional data was filtered with a lowpass Butterworth filter (sampling frequency 200 Hz, cutoff frequency 10 Hz). Many of the movements in the metabolic data collection were cut-off at the end before the movement was completed. To account for this, we use the last x-y position point and extend this for 0.5 seconds after the movement. X-Y position was then spline interpolated for two reasons. Position data was resampled at 400 Hz using spline interpolation. The center location, also where the hand starts, was set at x=-7.58 cm and y = 48.78 cm from the shoulder joint. Movement kinematics were taken from movement averages during the metabolic experiment and then used in the model. Average trajectories from each condition were low-pass 10 Hz filtered to create smooth trajectories.

Kinematic Validation

We wanted to determine if the model well replicated the desired movements. We took the simulated neural drive signals from the minimization procedure (minimizing active state squared), and then used a forward model to simulate the movement. We compare this simulated movement with the collected kinematic data. Figure S2 shows a comparison between the metabolic movement trajectories and simulated movement trajectories. The dashed lines represent the simulated movement, solid lines the average metabolic trajectory, and the shaded regions represent one standard deviation from the mean of the metabolic trajectories. We see that the model does a good job of recreating the movements. The different speeds are color coded with the faster speeds being darker (purple) with the slower speeds lighter (yellow). On average, subjects reached slightly further than 10 cm at the fastest speeds because subjects were not able to slow themselves to a stop for the fastest movements to rest at the target. Subjects tended to reach through the target and turn around at a distance past the target. This led to slightly longer movement durations than expected for the metabolic data for higher velocity reaches.

Step 2 - Inverse Kinematics

The second step converts the data (in x and y position data) to joint positions θ_e and θ_s and torques (τ_e, τ_s). These angles are defined by their Euler Angles and not flexion

Fig S2. Movement trajectories compared to model simulation using minimum jerk trajectories. Dashed lines represent the simulated movement, solid lines represent the average of the metabolic data, and shaded bars are one standard deviation from the mean. Each column from left to right is increasing in added mass to the hand (0 lbs, 5 lbs, 10 lbs, 20 lbs). The top row shows the distance from initial positions as a function of time. Bottom row is velocity as a function of time. The lines are color coded by the intended movement duration with darker (purple) representing shorter durations and lighter (yellow) lines longer movement durations.

extension angles. After determining the joint angles, we differentiate to get the angular velocities ($\dot{\theta}_e$ and $\dot{\theta}_s$) and accelerations ($\ddot{\theta}_e$ and $\ddot{\theta}_s$). In these equations l_1 and θ_s refer to the upper arm segment and shoulder joint. l_2 and θ_e refer to the forearm and elbow joint. A diagram of this system is shown in fig S3, $\theta_1 = q_1$ and $\theta_2 = q_2$.

We first define how endpoint position relates to joint positions in equation S1. Details can be found in multiple sources [63, 64].

$$\begin{aligned} \theta_e &= acos\left(\frac{x^2 - y^2 - l_1^2 - l_2^2}{2l_1 l_2}\right) \\ \theta_s &= atan2(y, x) - asin\left(\frac{l_2 sin(\theta_e)}{\sqrt{x^2 + y^2}}\right) \end{aligned} \tag{S1}$$

Step 3 - Inverse Dynamics

Arm Properties

We simulated the arm as a two link arm, the wrist was fixed during the experiment. The properties of the two links are shown in table S4. The masses and lengths of the arms were scaled to the height and mass of the subject and estimated using anthropomorphic measurements, such as fractions of body height and mass [29, 42]. The arm lengths and masses were similar to other studies [6, 65]. The centroid length of the arm segments are shown with 0 added mass, this distance was recalculated when mass was added. The center of mass length was estimated from Enoka [66].

In the biomechanical modeling equations, l_1 and θ_s refer to the upper arm segment and shoulder joint. l_2 and θ_e refer to the forearm and elbow joint. We then converted the data (in x and y position data) to joint positions θ_e and θ_s. These angles are defined by their Euler Angles and not flexion/extension angles. From there, we differentiated angular position to get the angular velocities ($\dot{\theta}_e$,$\dot{\theta}_s$) and accelerations ($\ddot{\theta}_e$,$\ddot{\theta}_s$). The beginnings of movements sometimes accelerated too fast for the model to replicate, so a small buffer was added to reduce acceleration for the first few time steps in the model. Last, an estimate for how the arm resists motion, the effective mass, was determined.

Object	Mass (kg)	Length (m)	$Cent_L$ (m)	I_{com}
Forearm	1.2500	0.4258	0.1674	0.0188
Upperarm	1.5909	0.3136	0.1367	0.0141

Table S4. Properties of the forearm and upperarm rigid segments for example subject of 56.81 kg and 1.62 m. The values for Forearm $Cent_L$ and I_{COM} are for 0 added mass at the hand. Centroid length is determined from the proximal joint.

Fig S3. Diagram for variables in the inverse dynamics of a two link arm using Euler angles and the Lagrangian Method [60].

Forearm Moment of Inertia

To find the new moment of inertia about the center of mass of the forearm plus added mass we need to use the parallel axis theorem. m_1 and m_2 refer to the masses of the upper arm and forearm respectively. $Cent_L$ refers to centroid length from proximal joint, with another subscript for before mass was added (old) and after mass is added (new).

$$\begin{aligned} Cent_{L,new} &= \frac{Cent_{L,old} \cdot m_2 + l_2 \cdot (\text{mass added})}{m_2 + \text{mass added}} \\ I_{com,new} &= 0.01882 + m_2(Cent_{L,old} - Cent_{L,new})^2 + \text{mass added}(l_2 - Cent_{L,new})^2 \end{aligned} \tag{S2}$$

Inverse Dynamics

To convert the joint angles into joint torques we need to apply the Lagrange-Euler equations of motion. The derivation of these equations can be found in many mechanics and dynamics textbooks. The final equations are shown in equation S3.

$$\begin{gathered} a_1 = m_1|^s x_{1c}|^2 +^2 I_1, a_2 = m_2|^s x_{2c}|^2 +^2 I_2,\ a_3 = m_2 l_1|^e x_{2c}|,\ a_4 = m_2 l_1^2 \\ \tau = \begin{bmatrix} \tau_s \\ \tau_e \end{bmatrix} = \begin{bmatrix} a_1 + a_4 + 2a_3 cos(q_2) + a_2 & a_2 + a_3 cos(q_2) \\ a_2 + a_3 cos(q_2) & a_2 \end{bmatrix} \begin{bmatrix} \ddot{q}_1 \\ \ddot{q}_2 \end{bmatrix} + \\ \begin{bmatrix} -a_3 \dot{q}_2 sin(q_2) & -a_3(\dot{q}_1 + \dot{q}_2 sin(q_2)) \\ a_3 sin(q_2)\dot{q}_1 & 0 \end{bmatrix} \begin{bmatrix} \dot{q}_1 \\ \dot{q}_2 \end{bmatrix} \end{gathered} \tag{S3}$$

After joint torques have been determined, the next step is to use musculoskeletal modeling to calculate the muscle properties and determine the force each muscle is required to output to produce the movement.

Effective Mass Calculation

The effective mass is used to estimate the arms resistance to a force in a given direction and represents m when parameterizing each effort representation as a function of time and mass [6]. The upperarm and forearm mass used in this calculation is scaled to the size of each subject using anthropomorphic estimates as fractions of body height and body mass [29, 42]. Effective mass is estimated by inducing a force of 1 in the reach direction to compute the effective mass of the reaching movement. In equation S4, θ is the angle of reaching direction, and +1 is added at the end to account for the inertia of the robotic arm manipulandum.

$$Effective\, mass = norm(M * \begin{bmatrix} cos(\theta) & sin(\theta) \end{bmatrix} + 1 \tag{S4}$$

The mass (M) matrix is defined as:

$$M = \left(\Lambda^{-1}\right)^T I(\theta) \Lambda^{-1} \tag{S5}$$

The mass matrix is computed from Jacobian matrix Λ (eq. S6) and the inertial matrix of the arm (eq. S7). In equations we define the variables as follows: $m_1 =$ upperarm mass, $r_1 =$ upperarm centroid length, $l_1 =$ upperarm length, $I_{COM,1} =$ moment of inertia about its center of mass. $m_2 =$ forearm mass, $r_2 =$ the length to the

center of mass of the forearm, r_{22} = the length to the centroid (arm + mass), l_1 = forearm length, $I_{COM,1}$ = moment of inertia about its centroid with the added mass.

$$\Lambda = \frac{dx}{d\theta} = \begin{bmatrix} -l_1 sin(\theta_s) - l_2 sin(\theta_s + \theta_e) & -l_2 sin(\theta_s + \theta_e) \\ l_1 cos(\theta_s) + l_2 cos(\theta_s + \theta_e) & l_2 cos(\theta_s + \theta_e) \end{bmatrix} \tag{S6}$$

$$I = \begin{bmatrix} m_1 r_1^2 + I_{COM,1} + (mass + m_2)(l_1^2 + r_{22}^2 + 2 l_1 r_{22} cos(\theta_e)) + I_{COM,2} \\ (m_2 + mass)(r_{22}^2 + l_1 r_{22}^2 cos(\theta_e)) + I_{COM,2} \\ (m_2 + mass)(r_{22}^2 + l_1 r_{22}^2 cos(\theta_e)) + I_{COM,2} \\ m_2 r_2^2 + mass \cdot l_2^2 + I_{COM,2} \end{bmatrix} \tag{S7}$$

Step 4 - Muscle Properties

Once joint torques were determined, we implemented an eight-muscle actuator model to match the computed joint torques. The muscle forces were calculated by distributing the force according to one of many (9) possible minimization functions representing some neuromechanical proxies (muscle force, muscle stress, active state, neural drive) for effort and one metabolic representation (Umberger 2010). Active state, an estimation of the percent of muscle activated, is calculated by simulating the properties of the muscles and estimating the portion of the muscle required to be active to match the torque. Neural drive, control signal from the central nervous system, is calculated from activation dynamics and the rate of change in active state. At each time step, the current active state and a neural drive of 1 and 0 are used to calculate the minimum and maximum possible active states at the next time point. This minimum and maximum active state are used as bounds for the muscle force allocation of the next time point. This process would repeat for each time step until the reach completed.

Muscles' properties of the eight simulated muscle actuators are shown in table S5 (mass, physiological cross-sectional area, optimal length, and percent fast twitch fibers). The eight muscles simulated are the anconeus (an), brachioradialis (br), brachialis (bs), biceps brachii (bb), clavicle portion of the pectoralis (pc), deltoid anterior (da), deltoid posterior (dp), and the triceps brachii (tb). Estimated muscle masses were computed by multiplying the optimal length by cross section area then multiplying by muscle density ($\rho = 10.6\ kg/m^3$). The physiological cross-sectional area (PCSA) for each muscle was estimated from cadaver studies or other models [67, 68, 69, 70, 71]. Our PCSA is slightly different than reported in literature but close. We altered some of the PCSA characteristics to more closely match total isometric torque output [72]. Holzbaur et al. report shoulder abduction of 54.7 Nm, shoulder adduction of 67.8 Nm, elbow flexion of 55.7 Nm, and 42.8 Nm for elbow extension. Our chosen PCSA leads to shoulder abduction of 54.28 Nm, shoulder adduction of 68.72, elbow flexion of 53.39 Nm, and elbow extension of 44.78 Nm. Optimal lengths were taken from multiple cadaver studies [73, 68, 71]. The optimal length of the anconeus and pectoralis muscles were set to occur at a shoulder flexion angle of 45^o as the anconeus muscle did not have values listed and we only used the clavicle portion of the pectoralis. Kistemaker et al. shows that the optimal elbow flexor angle to maximize the elbow moment is also 90^o [74]. The lengths of the muscles are determined by Pigeon et al, which models the muscle lengths and moment arms using cadaver studies and a polynomial equation [75]. The percent fast twitch of the eight muscles was estimated from Dahmane et al. and Johnson et al. [76, 77]. For data that is listed as deep and superficial portions, percent fast twitch is averaged between the deep and superficial muscle and used in the model.

Muscle	Mass (kg)	PCSA (m^2)	L_{OPT}	% FT
Anconeus (AN)	0.0095	1.3e-4	0.0687 (E)	40.0
Brachialis (BS)	0.0735	7.71e-4	0.090 (C)	40.0
Brachioradialis (BR)	0.0230	1.15e-4	0.1887 (L)	60.2
Deltoid Anterior (DA)	0.0887	6.46e-4	0.1296 (L)	42.9
Deltoid Posterior (DP)	0.0578	3.00e-4	0.1818 (L)	42.9
Pectoralis (PC)	0.0742	6.07e-4	0.1701 (E)	57.0
Biceps Brachii(BB)	0.0752	3.32e-4	0.225 (M)	53.6
Triceps Brachii (TB)	0.3408	9.94e-4	0.3235 (M)	52.9

Table S5. Muscle Properties. For L_{OPT}, the letter corresponds to which author the value was taken from or if it was estimated. C [73], L [68], M [71], E (estimated).

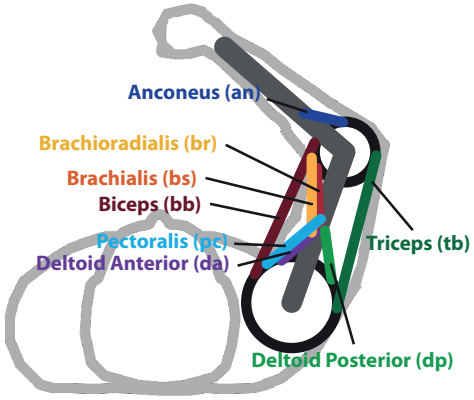

Fig S4. Diagram of the 8 simulated muscles and which muscles they represent.

PCSA, Optimal Length, and %FT

The muscle masses can be computed using $mass = L_{OPT} \cdot PCSA \cdot \rho$ where ρ is $10.6\,kg/m^3$ (ρ taken from [78, 79]. The PCSA for each muscle is estimated from Langenderfer et al. except for the anconeus which is from Holzbaur et al. [68, 80]. The $PCSA$ for each muscle can be estimated similar to the Todorov model [17], or from cadaver studies done by Holzbaur and Murray by dividing the muscle volume by the optimal fiber length [69, 71].

Currently the model uses the optimal muscle lengths from Murray [71] and combining the heads of muscles. Some of these values are taken from Langenderfer [68] as Murray does not test them. However, Chang et al. [73] shows that the optimal lengths of the muscles are quite a bit shorter than reported by Lagenderfer and Murray. I think the optimal muscle lengths for the brachialis should agree more with the shorter values in Chang [73] as these values match up closer to Pigeon [75] and Van Zuylen [81].

If not listed, the model assumes the optimal fiber lengths occur at 45° shoulder flexion and 90° elbow flexion, and that the length of the muscle at that position is given in equation S8. This method may not be accurate for some muscles as they would vary greatly if the equation is used when compared to the Langenderfer model [68]. Kistemaker shows 5 references that show that the optimal elbow flexor angle to maximize the elbow moment is also 45° [74].

Percent fast twitch of each of the muscles can be estimated from [76, 77]. For data that has deep and superficial values an average is taken for percent fast twitch.

Muscle Moment Arms

The moment arms were set to vary with shoulder an elbow position as defined below [75]. A negative moment arm is used to provide a negative torque around the joint as muscle force can never be less than 0.

The Pigeon model fits polynomials to the moment arm and muscle lengths as a function of shoulder and elbow angle. A graph showing how the moment arms are changing is shown in figure S5a.

$$\begin{aligned} MA &= x_n q_j^n + x_{n-1} q_j^{n-1} + \cdots + x_1 q_j + x_0 \\ ML &= cst + \sum_{j=1}^{3} (Y_n q_j^n + y_{n-1} q_j^{n-1} + \cdots + y_1 q_j) \end{aligned} \tag{S8}$$

The coefficients for this equation is shown in the tables below. Most of the coefficients are scaled to a power of 10.

Moment Arm Coefficients

DF	Elbow flexion/extension						Shoulder F/E
Muscle	$c_5 \times 10^9$	$c_4 \times 10^7$	$c_3 \times 10^5$	$c_2 \times 10^3$	$c_1 \times 10^1$	c_0	d_0
AN	-2.7306	10.448	-14.329	8.4297	-2.2841	-5.3450	
BS			-2.0530	2.3425	2.3080	5.5492	
BR			-6.5171	10.084	1.6681	19.490	
DA							33.02
DP							-78.74
PC							50.80
BB			-2.9883	1.8047	4.5322	14.660	29.21
TB	-3.5171	13.277	-19.092	12.886	-3.0284	-23.287	-25.40

Table S6. Coefficients for polynomial fits to moment arm lengths.

Muscle Lengths

The following equations describe how I calculate the lengths of the muscles. They are solved for in a similar way to moment arms [75]. A graphical representation of the muscle lengths is shown in figure S5b.

Muscle Length Coefficients

DF		Elbow flexion/extension						Shoulder F/E
Muscle	cst(mm)	$t_6 \times 10^1 1$	$t_5 \times 10^8$	$t_4 \times 10^7$	$t_3 \times 10^5$	$t_2 \times 10^3$	$t_1 \times 10^2$	$u_1 \times 10^1$
AN	53.57	4.7658	-1.8235	25.008	-14.713	3.9865	9.3288	
BS	137.48			3.5832	-4.0884	-4.0282	-9.6852	
BR	276.13			11.374	-17.600	-2.9114	-34.017	
DA	172.84							-5.7631
DP	157.64							13.743
PC	155.19							-8.8663
BB	378.06			5.2156	-3.1498	-7.9101	-25.587	-5.0981
TB	260.05	6.1385	-2.3174	33.321	-22.491	5.2856	40.644	4.4331

Table S7. Coefficients for polynomial fits to moment arm lengths.

The optimal lengths of the muscles as shown in table S5 and are estimated with the arm in a neutral position where $\theta_s = 45°$ and $\theta_e = 90°$ if data from literature couldn't be found.

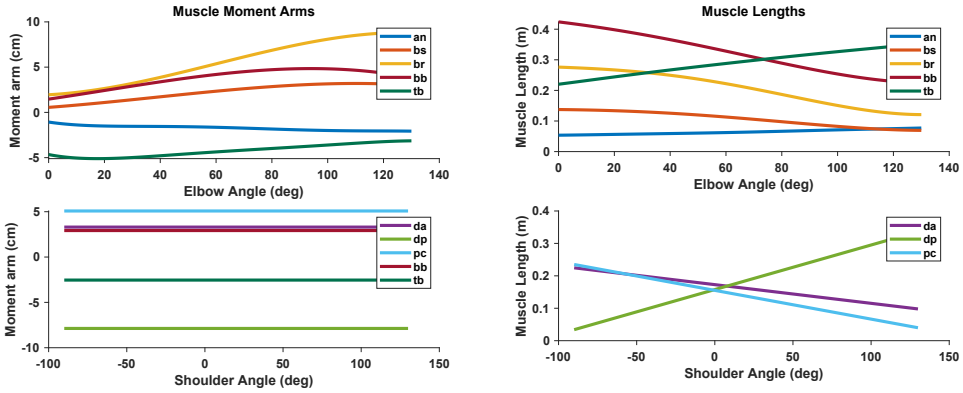

(a) Muscle moment arms as a function of shoulder or elbow angle.

(b) Muscle lengths as a function of joint angle (deg).

.

Fig S5. Muscle moment arms and lengths.

Int 1 - Cost Function Minimization

There are many possible minimization functions to distribute muscle forces due to the mechanical redundancy of the musculoskeletal system. Here we test 9 possible minimization functions, many shown on the left side of the flow chart (step Int-1). We test objective functions of stress, stress squared, muscle force, muscle force squared, active state, active state squared, neural drive, neural drive squared, and minimizing the Umberger model [19].

Int 2 - Muscle force bounds

Our model bound the active start of the muscle to a minimum of 0 and a maximum of 1. This is achieved by computing the minimum and maximum at every time point through the activation dynamics from the previous time point. The active state of the previous time point is fed a neural drive of either 0 or 1 to estimate the minimum and maximum active state at the current time point. This is done for every muscle at every time point to keep the active state between 0 and 1.

Step 6 - Active State Estimation

Once muscle force and muscle properties were calculated, we then estimated the active state of the muscles by simulating a modified Hill-type muscle [43]. This model estimates how much force a muscle can produce depending on the portion of muscle active and the muscle properties. The tendon (series elastic element) is set to be constant length and seems to be a reasonable approximation to make for low forces [82, 30, 83, 37, 84, 46].

Force-length/velocity properties

The model used is the Brown, Cheng and Loeb model to estimate the force length/velocity properties [43]. Other models can also be used such as cross-bridge cycling models [85, 86] or hill type models [87, 74, 88, 89, 90]. The Brown model accounts for active and passive elements of the muscle tendon unit. l is defined as the normalized length l/l_{OPT}, v is in normalized units of L_{OPT}/s. Activate state (a) is computed using Eq. S10. $F_{p,1}$ is the passive force resisting tension. $F_{p,2}$ is the passive

force resisting compression of the muscle. The tendon (series elastic element) is assumed to be constant length, thus providing no stretched force, and seems to be a reasonable approximation to make [82, 30, 83, 37, 84, 46].

The basic form of these equations is

$$\begin{aligned} F_{PE} &= F_{p,1} + R * A_f * F_{p,2} \\ F_{CE} &= R * A_F * F_L * F_V \\ F_{total} &= F_{PE} + F_{CE} \end{aligned} \tag{S9}$$

Which simlifies to

$$F_{total} = F_{p,1} + R * A_f(F_L * F_V + F_{p,2})$$

$$\begin{aligned} F_{p,1} &= 68.35 * 0.0495 * log(exp((l - 1.445)/(0.0495)) + 1) \\ F_{p,2} &= -0.02exp(13.8 - 18.7l) \\ F_v &= \begin{cases} \frac{-5.72-v}{-5.72+v(1.38+2.09l)} & v \leq 0 \\ \frac{0.62-v(-3.12+4.21*l-2.67l^2)}{0.62v} & v > 0 \end{cases} \\ F_l &= exp\left(-\left|\frac{l^{1.93}}{1.03}\right|^{1.87}\right) \\ N_f &= 2.11 + 4.16(\frac{1}{l} - 1) \\ A &= \frac{T - Fp,1}{F_l F_v + F_{p,2}} \\ a &= 0.56 N_F 10^{log_{10}(1-A)/N_f} \end{aligned} \tag{S10}$$

The passive force is subtracted from the total joint torque to solve for the active components of force that the muscles need to produce. Once the active state is calculated, it is scaled by a normalizing factor ($\sigma = 210Nm$ N/m^2) to calculate muscle force. This value was chosen to reasonably match maximum shoulder and elbow flexion torques [72]. This model produces, at elbow angle of 90^o and shoulder angle of 45^o, a maximum elbow flexion of 59 Nm, elbow extension of 47 Nm, shoulder flexion of 65 Nm, and shoulder extension 73 Nm.

$$F = a \cdot \sigma \cdot A, \qquad \text{where A is area} \tag{S11}$$

The passive force properties of the muscles seem to line up well with Horowits [91]. He reports at long sarcomere lengths the human muscles produce about 0.2-0.3 kg/cm^2. The biceps bracchii at its longest length was producing 0.35 kg/cm^2 passively.

Step 7- Activation Dynamics

After active state is estimated, a first order differential equation is used to calculate neural drive that estimates the active state rate as a function of neural drive [17, 20]. The active state is estimated from neural drive by passing u (neural drive) through a filter that describes calcium dynamics and cross-bridge cycling [17]. It is approximated using a first order non-linear filter. This is similar to other methods [45, 44, 43, 46].

$$\begin{aligned} \dot{a} &= \frac{(1 + \sigma_u \epsilon)u - a}{t(u, a)} \\ t(u, a) &= \begin{cases} t_{deact} + u(t_{act} - t_{deact}) & u > a \\ t_{deact} & otherwise \end{cases} \end{aligned} \tag{S12}$$

σ and ϵ represent noise in the neural drive signal. Currently I have 0 zero noise added to the signal. $t_{ACT} = 50$ msec, and $t_{DEACT} = 66$ msec. Using our muscle parameters of %FT we would get activation and deactivation times shown in table S8.

Muscle	%FT	t_{ACT}(ms)	t_{DEACT}(ms)
1	50.3	56.36	61.83
2	42.9	59.84	65.98
3	53.6	54.81	59.98
4	64.7	49.59	53.77
5	54.5	54.39	59.48
6	64.7	49.59	53.77

Table S8. Activation and deactivation times using the Umberger Model

Step 8 - Metabolics Models

Umberger Model 2003

One of the most prevalent models is the Umberger energy model [20, 19, 51]. This model assumes that there is some heat rate ($\dot{E}$) associated with the activation (h_A), maintenance (h_M), shortening/lengthening (h_{SL}), and work ($\dot{w}$) done by the muscle that when added together is equal to the total energy rate ($\dot{E}$) shown in eq. S13.

$$\dot{E} = \dot{h}_A + \dot{h}_M + \dot{h}_{SL} + \dot{w}_{CE} \tag{S13}$$

Activation and maintenance heat rate, h_{AM}

The activation and maintenance are often grouped together into one term, h_{AM}. Scaling factors are added to account for the length and activation dependence of $\dot{h}_{AM}$ and $\dot{h}_{SL}$. $\dot{h}_{AM}$ and $\dot{h}_{SL}$ are scaled by the normalized, isometric force-length relation (F_{iso}) when $L_{CE} > L_{CE(OPT)}$.

We define h_{AM} below, this value will be scaled by the factors above depending on the length and velocity of the muscle (eq. S14).

$$\dot{h}_{AM} = 1.28 \times \%\text{FT} + 25 \tag{S14}$$

To get appropriate activation dependence a scaling factor (A) that depends on STIM and ACT is defined:

$$A = \begin{cases} STIM & \text{when } STIM > ACT \\ (STIM + ACT)/2 & \text{when } STIM \leq ACT \end{cases} \tag{S15}$$

Then for scaling $\dot{h}_{AM}$ and $\dot{h}_{SL}$ we define:

$$\begin{aligned} A_{AM} &= A^{0.6} \\ A_{SL} &= A^{2.0} \end{aligned} \tag{S16}$$

$\dot{h}_{SL}$ is scaled by A_{SL} when $\tilde{V}_{CE} \leq 0$ and by A when $\tilde{V}_{CE} > 0$.

Shortening and lengthening heat rate, h_{SL}

This model uses a modified Hill-Type model. It was modified to better account for force production at submaximal activation and the effects of between-muscle fiber type differences. These are based on a hill type model of the muscle that consists of a contractile element(CE) and a series elastic element (SEE).

The normalized hill constants $A_{REL}(= a/F_{MAX})$ and $B_{REL}(= b/L_{CE(OPT)})$ determine the shape of force-velocity curve and maximal shortening velocity (and power that can be generated given maximal isometric force (F_{MAX})). When multiple muscles are modeled simultaneously, a common approach is to assign all muscles same normalized Hill-constants. Here, they scale A_{REL} and B_{REL} by the percent of type II fibers.

$$\begin{aligned} A_{REL} &= 0.1 + 0.4(\%FT/100) \\ B_{REL} &= A_{REL}\tilde{V}_{CE(MAX)} \end{aligned} \tag{S17}$$

$\tilde{V}_{CE(MAX)}$ is the maximum shortening velocity of the muscle relative to its length. In these constants, $\tilde{V}_{CE} = V_{CE}/L_{CE(OPT)}$, and is expressed in $L_{CE(OPT)}s^{-1}$. A value of 12 $L_{CE(OPT)}s^{-1}$ is used for $\tilde{V}_{CE(MAX)}$.

Shortening heat coefficients for slow twitch and fast twitch fibers:

$$\alpha_{S(ST)} = \frac{4 \times 25}{\tilde{V}_{CE(MAX-ST)}}$$
$$\alpha_{S(FT)} = \frac{1 \times 153}{\tilde{V}_{CE(MAX-FT)}} \tag{S18}$$

For these coefficients, $\tilde{V}_{CE(MAX-FT)}$ is defined by the Hill coefficients A_{REL} and B_{REL}. $\tilde{V}_{CE(MAX-FT)}$ is assumed to be 2.5 times greater than $\tilde{V}_{CE(MAX-ST)}$

Combining these equations, we get the shortening heat rate:

$$\dot{h}_{SL} = -\alpha_{S(ST)}\tilde{V}_{CE}(1 - \%FT/100) - \alpha_{S(FT)}\tilde{V}_{CE}(\%FT/100) \qquad \text{for } \tilde{V}_{CE} \leq 0 \tag{S19}$$

The rate of extra heat production in lengthening can be represented as a product of a coefficient α_L and CE velocity, with a slope slightly greater than shortening.

$$\alpha_L = 4\alpha_{S(ST)} \tag{S20}$$

Where $\alpha_{S(ST)}$ is defined in equation S18. We then get the heat rate for a lengthening muscle.

$$\dot{h}_{SL} = \alpha_L \tilde{V}_{CE} \qquad \text{for } \tilde{V}_{CE} \geq 0 \tag{S21}$$

Mechanical Work Rate, $\dot{w}$

Mass specific mechanical work rate is given by:

$$\dot{w}_{CE} = -\frac{F_{CE}V_{CE}}{m} \tag{S22}$$

Where m is the mass of the muscle.

Total work rate

The parameters $\dot{h}_{AM}$, $\dot{h}_{SL}$, $\dot{w}$ are all scaled by the parameters above depending on the length and velocity of the muscle while contracting to get an estimate for the total energy rate. The total energy liberation for a muscle in W/kg (total muscle mass) is:

$$\begin{aligned} &\text{if } L_{CE} \leq L_{CE(OPT)} \\ &\dot{E} = \dot{h}_{AM}A_{AM}S \\ &\quad + \begin{cases} [-\alpha_{S(ST)}\tilde{V}_{CE}(1 - \%FT/100) - \alpha_{S(FT)}\tilde{V}_{CE}(\%FT/100)] \cdot A_S S & \text{if } \tilde{V}_{CE} \leq 0 \\ \alpha_L \tilde{V}_{CE} AS & \text{if } \tilde{V}_{CE} > 0 \end{cases} \\ &\quad - (F_{CE}V_{CE})/m \end{aligned} \tag{S23}$$

$$\begin{aligned} &\text{if } L_{CE} > L_{CE(OPT)} \\ &\dot{E} = (0.4 \times \dot{h}_{AM} + 0.6 \times \dot{h}_{AM}F_{ISO}A_{AM}S) \\ &\quad + \begin{cases} [-\alpha_{S(ST)}\tilde{V}_{CE}(1 - \%FT/100) - \alpha_{S(FT)}\tilde{V}_{CE}(\%FT/100)]F_{ISO}A_S S & \text{if } \tilde{V}_{CE} \leq 0 \\ \alpha_L \tilde{V}_{CE} F_{ISO} AS & \text{if } \tilde{V}_{CE} > 0 \end{cases} \\ &\quad - (F_{CE}V_{CE})/m \end{aligned} \tag{S24}$$

2010 Model

In 2010, a slight alteration to the model was made to better account for the actual ATP cost during lengthening by excluding negative CE work from the summation by redefining the lengthening heat rate coefficient (α_L) [19]. Equation S25 shows the new relation, which is then used in the full metabolic model above (eq. S23).

$$\alpha_L = 0.3\alpha_{S(ST)} \tag{S25}$$

Bhargava Model 2004

Following suit of Umberger, this model estimates the metabolic rate of the muscle from the activation, maintenance, shortening, and basal heat rate [21]. Bhargava collected heat data on frog sartorius muscles, then used a walking model to estimate energetics to evaluate the model. The total energy is divided into five energy terms

$$\dot{E} = \dot{A} + \dot{M} + \dot{S} + \dot{B} + \dot{W} \tag{S26}$$

where $\dot{A}$ is the activation heat rate, $\dot{M}$ is the maintenance heat rate, $\dot{S}$ is the shortening heat rate, $\dot{B}$ is the basal metabolic rate, and $\dot{W}$ is the work rate.

The activation heat as with the others represents the heat produced by stimulation of the muscle and is primarily due to Ca^{2+} ion movement. The activation heat is broken into two terms, one for fast twitch fibers and another for slow twitch fibers.

$$\dot{A} = \phi m f_{fast} \dot{A}_{fast} u_{fast}(t) + \phi m f_{slow} \dot{A}_{slow} u_{slow}(t) \tag{S27}$$

m is the total mass of the muscle, f_{fast} and f_{slow} are the fractions of the muscle that are labeled as fast or slow twitch, $\dot{A}_{fast}$ and $\dot{A}_{slow}$ are the activation heat rate constants for fast and slow twitch fibers. In equation S27, ϕ is a decay function that models observed heat production where most of the heat is produced at the beginning of activation and decays over time to 6% of the initial level with a time constant of 45 ms.

$$\phi = 0.06 + e^{-t_{stim} u(t)/\tau_\phi} \tag{S28}$$

where τ_ϕ is the time constant (45 ms), t_{stim} is the amount of time the muscle is excited about 10%.

$u_{fast}(t)$ and $u_{slow}(t)$ are the excitation levels of the fast and slow twitch fibers. A single input $u(t)$ is used for the entire muscle, so a conversion is used to separate into $u_{fast}(t)$ and $u_{slow}(t)$.

$$\begin{aligned} u_{fast}(t) &= 1 - cos(\pi/2 * u(t)) \\ u_{slow}(t) &= sin(\pi/2 * u(t)) \end{aligned} \tag{S29}$$

Bhargava argues that these generally represent the size principle within muscles, that at low levels of excitation only the small fibers will be recruited and at high levels of excitation both fibers will be recruited.

The maintenance hate rate is split into two terms as well, one for fast twitch and one for slow twitch.

$$\dot{M} = L(\tilde{l}^M) m f_{fast} \dot{M}_{fast} u_{fast}(t) + L(\tilde{l}^M) m f_{slow} \dot{M}_{slow} u_{slow}(t) \tag{S30}$$

$\dot{M}_{fast}$ and $\dot{M}_{slow}$ represent the hate rate constants for fast and slow fibers, $L(\tilde{l}^M)$ is a function describing the dependence on muscle length. $L(\tilde{l}^M)$ is modeled by a piece-wise function of normalized muscle fiber length (fig S6). At very long lengths, the

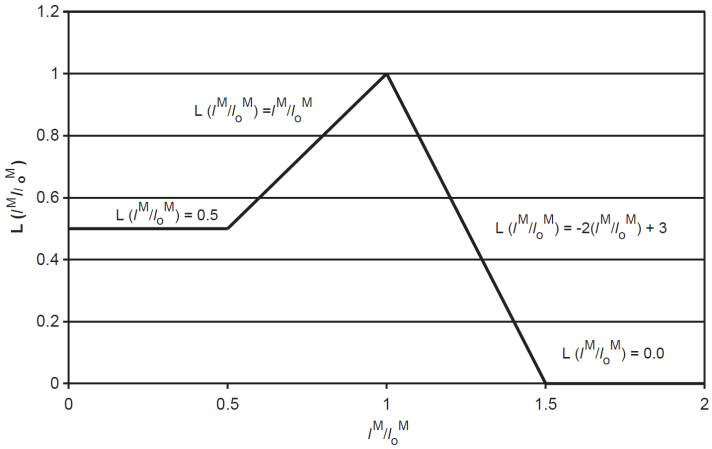

Fig S6. Maintenance heat rate depends on length and is used in equation S30. This graph is from Bhargava [21].

muscle uses no heat for maintenance because there is no overlap of action-myosin, and ant very low lengths the overlap does not change so a constant maintenance heat rate is applied.

The shortening heat rate is related the velocity of shortening by

$$\dot{S} = -\alpha v_{CE} \tag{S31}$$

where α is a proportionality constant, and v_{CE} is the velocity of the contractile element in the hill type model. The parameter α is dependent on the velocity of the contractile element.

$$\alpha = \begin{cases} 0.16F^M_{iso}(a(t), l^M) + 0.18F^M, & \text{if } v_{CE} \leq 0 \\ 0.157F^M, & \text{if } v_{CE} > 0 \end{cases} \tag{S32}$$

The basal rate of the muscle is just a scalar of the mass of the muscle

$$\dot{B} = 0.0225m \tag{S33}$$

where m is the mass of the muscle.

The last component, $\dot{W}$ is the force of the contractile element (F_{CE}) multiplied by the shortening velocity (V_{CE}). F_{CE} is determined from the activation, force length, and force velocity properties of the muscle (S1).

$$\dot{W} = F_{CE}(l_{CE}, v_{CE}, a(t))v_{CE} \tag{S34}$$

Parameter values for $\dot{A}_{fast}, \dot{A}_{slow}, \dot{M}_{fast}, \dot{M}_{slow}, l^M_0, F^M_0$ can be found in Bhargava [21].

Lichtwark Model 2005

In a similar fashion to the previous models, Lichtwark modeled the heat rate of the muscles based off the mechanical efficiency of the muscles [24]. This model breaks the rate of heat production into four functions that when added together produce the total heat rate.

$$\frac{dH}{dt} = \frac{dH_M}{dt} + \frac{dH_L}{dt} + \frac{dH_S}{dt} + \frac{dH_T}{dt} = f(Act) + f(Act, t) + f(Act, V_{CE}) + f(P) \tag{S35}$$

where H_M is the stable (maintenance) heat rate, H_L is the labile heat rate, H_S is the shortening heat rate, H_T is the thermoelastic heat rate, P is the relative force produced, Act is the activation level, V_{CE} is the velocity of the contractile element.

H_M is the heat rate to produce isometric force for a given activation state. This has been shown to be well approximated by multiplying the Hill type force-velocity constants $a \times b$. The relationship for H_M is then defined as

$$\frac{dH_M}{dt} = Act\left(\frac{a}{P_0} \times \frac{b}{V_{max}} \times \frac{V_{max}}{L_0}\right) = Act\left(\frac{V_{max}}{G^2}\right) \tag{S36}$$

where $G = P_0/a = V_{max}/b$ and V_{max} is the maximum shortening velocity. a and b are determined from the normalization constants of the hill-type model. These can be determined in a similar manner to the Umberger model (sec S1) and are further described by Winters and Stark [92, 20]. P_0, L_0 are used for normalizing the units.

When a muscle contracts over time, the maintenance heat rate can decay in an exponential fashion to about 2-3x, and this is termed labile heat. Knowing this the liable heat rate can be defined as

$$\frac{dH_L}{dt} = 0.8\frac{dH_M}{dt}e^{-0.72t} + 0.175\frac{dH_M}{dt}e^{-0.022t} \tag{S37}$$

The shortening heat rate relates the cost to shortening a muscle for a given activation level. The following equation relates the shortening velocity to the heat rate only when the muscle is shortening.

$$\frac{dH_s}{dt} = Act\left(\frac{a}{P_0} \times \frac{V_{CE}}{L_0}\right) = Act\left(\frac{V_{CE}}{G}\right) \tag{S38}$$

In eccentric contractions energy cost is generally lower than concentric or isometric contractions. This model assumes that during active lengthening that the minimum heat rate must be 30% of the stable heat rate [93]. There is also an exponential decay of energy production as lengthening velocity increases [94]. The rate of heat during a lengthening contraction is approximated by

$$\frac{dH_S}{dt} = 0.3\frac{dH_M}{dt} + 0.7\left(\frac{dH_m}{dt}e^{-8\left[\frac{P}{Act}-1\right]}\right) \tag{S39}$$

The last component accounts for the heat absorbed by the muscle, which is proportional to the rate of force production.

$$\frac{dH_T}{dt} = -0.014\frac{dP}{dt} \tag{S40}$$

These components are combined with the input parameters (F, L_{CE}, Act, V_{max}, G) to create the full model for energy expenditure

$$\begin{aligned}\frac{dH}{dt} =& Act\left(\frac{V_{max}}{G^2}\right) \\ &+ 0.8\frac{dH_M}{dt}e^{-0.72t} + 0.175\frac{dH_M}{dt}e^{-0.022t} \\ &+ \begin{cases} Act\left(\frac{V_{CE}}{G}\right) & \text{if } V_{CE} > 0 \\ 0.3\frac{dH_M}{dt} + 0.7\left(\frac{dH_m}{dt}e^{-8\left[\frac{P}{Act}-1\right]}\right) & \text{if } V_{CE} < 0 \end{cases} \\ &- 0.014\frac{dP}{dt}\end{aligned} \tag{S41}$$

Uchida Model 2016

The Uchida model takes components form the Umberger model and Bhargava model to create a new model [23]. The primary aspects of this model are the same as the Umberger model, where the only changes are how this model handles muscle excitation and negative power.

Uchida uses the excitation model of Bhargava to create orderly recruitment of muscle fibers [21].

$$\begin{aligned} u_{slow}(t) &= sin(\frac{\pi}{2}u(t)) \\ u_{fast}(t) &= 1 - cos(\frac{\pi}{2}u(t)) \\ f_{slow}^{rec}(t) &= \begin{cases} 1, & \text{if } u(t) = 0 \\ \frac{f_{slow}u_{slow}(t)}{f_{slow}u_{slow}+(1-f_{slow})u_{fast}(t)}, & \text{otherwise} \end{cases} \end{aligned} \tag{S42}$$

$u(t)$ is the muscle excitation level, $u_{slow}(t)$ and $u_{fast}(t)$ are the broken-down components of $u(t)$ into slow and fast twitch fibers, f_{slow} is the fraction of slow twitch fibers within the muscle, and $f_{slow}^{rec}(t)$ is the fraction of the fibers recruited that are slow twitch. This allows for different energetics models based on the fiber type and properties within the model.

The second change Uchida made to the Umberger model is how negative mechanical work is dealt with. The 2003 Umberger model included negative mechanical work, but was revised in the 2010 model [20, 19]. Negative work accounts for much of the differences in some energetics models [13]. During eccentric contractions, the muscles were allowed to absorb energy in the Uchida model if the negative mechanical work rate exceeded the total positive heat rate in a similar fashion to the 2003 Umberger model. Instead of returning this energy to the muscle however as the chemical reactions cannot be easily reversed in the muscle, the absorbed energy was immediately dissipated as heat. This prevents the total instantaneous power being less than zero.

The average power for each muscle was calculated by integrating the energy, and normalizing to muscle mass.

$$P_{avg} = \frac{m}{t_1 - t_0}\int_{t_0}^{t_1} \dot{E}(t)dt \tag{S43}$$

Margaria 1968

The Margaria model [40] estimates the metabolic rate assuming that muscles are 25% efficient when shortening and 120% efficient while lengthening:

$$\dot{E} = \begin{cases} \frac{\dot{w}}{0.25} & \text{if } v_{CE} < 0 \\ -\frac{\dot{w}}{1.20} & \text{if } v_{CE} \geq 0 \end{cases} \tag{S44}$$